A meta-analysis of fault slip rates across the central Apennines

M. M. C. Carafa[1]*, D Di Naccio[1], C. Di Lorenzo[1], V. Kastelic[1], P. Bird[2]

[1]Istituto Nazionale di Geofisica e Vulcanologia, Sezione di Sismologia e Tettonofisica, L'Aquila, Italy.

[2]University of California, Department of Earth, Planetary and Space Sciences, Los Angeles, US.

Corresponding author: Michele M. C. Carafa, michele.carafa@ingv.it.

Key Points:

- We meta-analyzed throw measurements for active normal faults in the central Apennines;
- Throw rates are overdispersed with respect to age and offset uncertainties; therefore, larger uncertainties are implied;
- A robust null hypothesis is that most faults have throw rates that are quasi-constant through geologic time, and also along their traces, except for tapering at unconnected ends.

Abstract

Several methods such as paleoseismic trenching, mapping of offset geomorphic markers, and dating of scarp profiles have been used to determine slip rates of normal faults in the central Apennines. Combining measurements obtained with different methods remains challenging because non-tectonic processes can introduce noise or spurious signals that are elusive to quantify, and these influence slip rate estimates. To this end, we meta-analyzed throw measurements with associated ages collected in the central Apennines with several methods to quantify such erratic fluctuations and method-related variances.

We show that throw rates are overdispersed with respect to nominal uncertainties in throw and age; therefore, they are commonly affected by unmodeled noise processes. After comparing throw rate distributions sampling the same faults with different techniques, no clear spatiotemporal patterns appear, but only quasi-random noise. Assuming that field investigators sampled real tectonic features (i.e., fault scarps), we find that such erratic throw rates indicate total uncertainties are two to three times greater than the stated observation uncertainties. In this situation, a simple and robust null hypothesis is appropriate. We propose that most faults should be assumed to have uniform throw rate along their traces, except for possible tapering near unconnected ends. We also propose that models in which throw rates are time-dependent (within the last 25 ka) are not yet justified. Then, relying on the estimated total uncertainties, we determine the most probable long-term fault throw rate for each active fault by combining different throw-rate probability density functions.

Plain Language Summary

Recent advances in paleoseismology are expected to provide crucial components for seismic hazard models in the years to come. Different paleoseismological methods sample complementary features along active fault traces. Thus, the most significant progress in seismic hazard analyses using paleoseismological data will stem from advanced statistical methods comparing (and connecting) outcomes of different techniques. However, comparing alternative techniques remains problematic, given the limited number of feature measurements across the same active fault.

The available data for active faults across the central Apennines, collected with diverse methods by different research groups, represents an opportunity to solve this issue due to their dense concentration. Furthermore, such data richness motivated us to carefully investigate the spatial and temporal variabilities to discriminate tectonic signals from noise.

We meta-analyzed available throw measurements (and their ages), inspected for disagreements among features, and found evidence for significant data overdispersion. Hence, we argue that better quantification of the total uncertainties is needed and that uniform throw rate (along each trace and

through the last 25 ka of geologic time) is still the most reasonable model for many scientific and urban planning purposes.

1 Introduction

Recent seismic hazard models are increasingly relying on fault slip rates as the fundamental quantity for translating the activity of a fault source model into earthquake rates (Field et al., 2014; Kastelic et al., 2016; Murru et al., 2020; Visini et al., 2021). In this conversion, modelers are often tasked with selecting different estimates and alternative methods to assess the fault slip rates and related uncertainties and incorporate them into the seismic hazard analysis.

As for the central Apennines, most fault estimates are restricted to the past 25 kyr. Considering that stable estimates can be retrieved after 5-10 earthquakes causing slip at the some point on some fault trace, this time interval is barely sufficient to assess reliable long-term slip rates because the recurrence interval for strong earthquakes on each fault is 1000-3000 yr (Galli, 2020).

A further complicating factor in determining long-term estimates is earthquake clustering. Episodic behavior has been suggested for the central Apennines, alternating thousands of years of rapidly accumulating displacement and similar periods of almost complete inactivity (Cowie et al., 2017). However, such clustering models are inconsistent with periodic and quasi-stationary slip rates reported for Mount Morrone (Gori et al., 2011), the Middle Aterno Valley fault (Falcucci et al., 2015), and other faults of central Apennines (Galadini & Galli, 2000).

The findings of different studies on the along-strike variation of throw rates in the central Apennines are also controversial and potentially misleading. There is increasing literature suggesting along-strike variation and even proposals to use specific model throw-rate profiles for exploratory seismic hazard assessments (Faure Walker et al., 2019). These data collections usually mimic the theoretical model of the along-strike throw distribution of a growing isolated (unconnected) fault in a uniform medium (Cowie & Scholz, 1992; Peacock & Sanderson, 1991) with variable throw rates. This model mainly relies on detailed field mapping of active faults and related slip rates. However, geologic mapping can report incomplete fault traces due to vegetation, grazing animals, plowing, urban development, soil creep, landsliding, or other non-tectonic processes that hide parts of the fault traces. Also, any strike-slip faults that may connect to the mapped ends of normal faults may remain undetected because they produce no scarps.

Furthermore, it has been proven that climate change, topographic gradients, and the vertical and lateral variation of geotechnical properties play crucial roles in unevenly amplifying, or possibly reducing, the throw along fault traces. These sources of noise are active both in interseismic (Kastelic et al., 2017;

Stemberk et al., 2019) and coseismic phases, both in the Apennines (Di Naccio et al., 2019) and elsewhere (Chen et al., 2012; Roback et al., 2018). As a result, the measured slip rate fluctuations can reflect the influence of different noise sources reshaping the fault scarps more than a real (tectonic) variation of long-term slip rate along the trace. This implies that the observational errors in throw measurement at each single site might not capture the lateral overdispersion of throw measurements. Thus, short-wavelength non-tectonic variations require an epistemic uncertainty in slip rate estimates about three times bigger than the observational error (McPhillips & Scharer, 2018).

Several "static" models of seismogenic sources (Basili et al., 2008; Boncio et al., 2004) have been proposed as an alternative to the growing-fault models because they relax the assumption of fitting, and locally overshooting, the throw rates along the fault strike. Despite significant procedural differences, these static models define a main fault ("seismogenic master fault" Boncio et al., 2004) or "composite seismogenic source" (Basili et al., 2008) with a constant slip rate in space and time, but tapering to zero at any unconnected fault tips. These major structures are considered continuous at depth, although they might split into closely spaced fault segments at the surface.

Finally, different methods have been applied in the central Apennines to quantify fault slip rates. However, alternative methods sample complementary features, and examining fault activity with alternative techniques is expected to sample different spurious signals if non-tectonic processes are not marginal. Unveiling this latter point is fundamental for any modeler. Similarly, combining rates acquired with different methods remains the most challenging as an agreed method of synthesizing slip rates is still missing (Morell et al., 2020). Therefore, the central Apennines represent an optimal case study due to the temporal and spatial proximity of the relative measurement points of different methods. With this goal, we meta-analyzed available throw measurements (and their ages), inspected for disagreements among features, and found evidence for significant overdispersion among different techniques of throw measurement. Hence, additional epistemic uncertainties are implied, and they may be larger than observational uncertainties by a factor varying up to two/three for scarp profiling.

We warn against overfitting of throw rates, which invokes unsupported spatial or temporal fluctuations in the last 25 kyr, and argue that a uniform throw rate (tapering to zero at any unconnected fault tips) is still the most reasonable model for many scientific and urban-planning purposes.

2 Study area and geological background

Our study area extends for more than 150 km along the central Apennines (Figure 1). This mountain range was originally a northeast-verging fold and thrust belt, but now the axial portion is undergoing regional uplift and NE-SW active extension since Late Neogene-Early Quaternary (Carafa & Barba, 2013; Cavinato & Celles, 1999). Extension at 2.5-3.5 mm/a (Carafa & Bird, 2016; Carafa et al., 2020; Devoti et

al., 2017) shaped a complex landscape featuring previous thrust-belt ranges, glacial and fluvial landforms, karst plateaus, and fluviolacustrine basins. In the central Apennines, the NW-SE and NNW-SSE striking normal faults dissect and overprint older compressional features, drive the deposition in intramountain basins (e.g. Fucino and Sulmona basins), and control the Late Pleistocene (< 126 ka)-Holocene continental deposits and landforms. The average fault trace length is greater than 10 km, and these are usually interpreted as ground-breaking tectonic faults, although investigations along the strike and in-depth are scarce, and the role of exogenic processes perturbing the tectonic signal remains underexplored.

In many cases, the faults separate footwall carbonates from unconsolidated deposits such as slope debris and colluvium eluvium or alluvial fan deposits in the hanging wall (Blumetti et al., 1993; Galadini & Galli, 2000), and their trace is lost where the relief ends. In this setting, bedrock fault scarps are locally well-exposed and mapped at different elevations along the steep carbonate bedrock of the footwall. These latter features have been documented to favor slope instabilities mimicking a tectonic signal (Galadini, 2006; Kastelic et al., 2017). In other cases, fault planes are not visible at the ground surface, but they leave dislocated landforms and stratigraphic markers or earthquake horizons (Galli et al., 2008). Evidence of fault activity is supported by displaced Pleistocene and Holocene alluvial fans, slope deposits (Galli et al., 2010; Gori et al., 2007; Miccadei et al., 2002; Villani et al., 2015), and smooth upland surfaces mainly created around the time of the Last Glacial Maximum (Giraudi, 1995; Pantosti et al., 1996; Papanikolaou et al., 2005; Roberts & Michetti, 2004).

3 Review of applied methods to determine paleoearthquake throw and cumulative throw rate in the central Apennines

We collected the cumulative throw rates from a thorough literature review on geologic/geomorphic data along 59 normal fault traces in the central Apennines, also considering alternative versions of data contested by competing research teams.

In an extensional setting like the central Apennines, offsets are usually constrained by vertical separation of displaced stratigraphic layers or geomorphic features. For this reason, all of our performed calculations and results have been focused on the relative vertical offset (throw). We calculated the throw from slip (when necessary) using the reported dip angle in the few cases analyzing the offset along the fault plane (see Benedetti et al., 2013, as an example). The most common geomorphic markers used as piercing points to calculate fault offsets are fluvial terraces, alluvial-glacial fan surfaces, moraine crests, valleys, and remnants of peneplains. The offset age is bracketed by several Quaternary dating methods, such as radiocarbon and cosmogenic radionuclide. In many cases, the dislocation events are constrained by correlation with regional subplanar surfaces or stratigraphic layers of known age (Blumetti & Guerrieri, 2007; Galadini, 1999; Giraudi & Frezzotti, 1997). For different faults (e.g.

Aremogna-Cinque Miglia, Sangro-Mt. Marsicano, Barisciano-San Pio delle Camere, Campo Felice, Campo Imperatore, Assergi), we opted to analyze the throw rates of each splay and not merge them in a single polyline to highlight eventual spatial variations.

We organized the collected data into two different datasets. The first one (Table S1) contains 403 throw features older than 2 ka as younger rates can be affected by non-marginal elastic-strain changes (see section 4.3 "Definition and determination of the net elastic offset ΔE"). This dataset is meta-analyzed to determine the uniform throw rate along 59 normal faults. The second dataset (Table S2) contains all the dislocations resulting from single paleoearthquake throws (150 measurements) regardless of the age of the event as this allowed us to determine the distribution of coseismic throws along a set of 18 representative normal faults. This dataset is used to estimate the coseismic slip distribution of all active faults in the central Apennines (see section 4.3 "Definition and estimation of the net elastic throw ΔE").

We divided the cumulative throw rate measurements into four classes according to the used methodology.

3.1 Paleoseismic trenching (TRCH)

In the last three decades, paleoseismic trenching (from now on, the TRCH technique) identified several previously unknown paleo-earthquakes in the central Apennines (Boncio et al., 2010; Cinti et al., 2011; D'Addezio et al., 2001; Galadini & Galli, 1999; Michetti et al., 1996; Moro et al., 2013; Salvi et al., 2003; Saroli et al., 2008; Serva et al., 1986). Throw rates were measured for different studied faults by digging trenches in Quaternary continental deposits, mapping their walls, and determining earthquake displacements. In detail, paleoseismological trenches are focused on measuring earthquake horizons, defined as coseismic throws or deformed landforms and sediments. The dislocation measurements often represent minimum throw estimates due to previous erosional events altering the preservation of stratigraphic layers in the footwall. In other cases, layers are not recognizable within the hangingwall or are buried below it. Throw age is often bracketed between the age of the pre- and post-earthquake layers and has been determined by dating collected samples (e.g., shells, charcoal, paleosoils) or tephra layers by radiocarbon, thermoluminescence, and archeological methods. The total number of TRCH measurements is 46 in the throw rate dataset (Table S1) and 81 in the coseismic throw dataset (Table S2).

3.2 Measuring geomorphic markers post Last Glacial Maximum (LGMA method)

The Last Glacial Maximum (LGMA) extensively shaped the landscape resulting in erosive landforms (e.g., cirques or glacial valleys) and deposits (till, moraine, or glacial fans) on a regional scale (Giraudi, 1988, 1989, 1995). The last age at which these climate-induced features dominated over tectonic scarp-formation constrains the later cross-cutting activity of faults in the central Apennines. Last Glacial Maximum data refer to dislocated subplanar or sublinear geological and geomorphic markers exposed

since this climate change (Giraudi & Frezzotti, 1995; Piccardi et al., 1999; Roberts & Michetti, 2004). This data subset often lacks direct dating of the geomorphic marker because it assumes the observed offset has occurred since the demise of the Last Glacial Maximum (15±3 kyr, Faure Walker et al., 2010). Furthermore, investigators often believe that the sampled parts of the footwall and hangingwall slopes are intact because recent exogenic processes on faults scarps are not expected to perturb the tectonic signal (Tucker et al., 2011). Under this assumption, the scarp height variations along strike are purely tectonic features because they represent cumulative throws. With 232 data points, the LGMA is the most common sampling technique in our data collection. For many data, the offset is routinely estimated by the intersection of the fault scarp topography with the surrounding surface morphology with meter ruler accuracy, which define the observational error of the measurement (Bubeck et al., 2015; Cinti et al., 1992; Faure Walker et al., 2009; Faure Walker et al., 2010; Morewood & Roberts, 2000; Pizzi & Pugliese, 2004; Wilkinson et al., 2015).

3.3 Geochemical dating (CHEA method)

Dating methods deriving from measurements of terrestrial cosmogenic radionuclide concentrations in rocks and sediment are commonly used in geomorphic and neotectonic studies (Amos et al., 2007; Balco, 2011; Cyr & Granger, 2008; Darvill, 2013; Granger et al., 2013). In the central Apennines, the surface exposure dating techniques have been applied to footwall carbonates scarps to recover the fault slip histories and paleoearthquakes (Benedetti et al., 2013; Carcaillet et al., 2008; Schlagenhauf, 2009; Schlagenhauf et al., 2010; Tesson et al., 2016). This dating method relies on measuring the production of ^{36}Cl cosmogenic radionuclide due to cosmic ray-induced reactions often combined with the concentration of rare earth elements undergoing dissolution and recrystallization after their exhumation. Thus, the fault scarp exposure at a specific site is recovered by modeling the geochemical element concentration from the top to the base of the fault ribbon and several meters below the ground surface. The variation of geochemical concentration is then linked to the fault slip history at the measurement point under the assumption of hangingwall wedge stability and absence of hillslope processes, as for LGMA method. We will refer to this method as CHEA and 73 measurements were collected in the throw rate dataset (Table S1) and 69 in the coseismic throw dataset (Table S2).

3.4 Measuring long-term (>20 ka) markers (LONG class)

All these three techniques investigate the cumulative throw of the past 20 kyr. For the estimates relying on greater feature ages, we defined the long-term (LONG) class. Generally, they consist of dislocated geological/geomorphologic markers and the reported features are suspended high on the footwall and correlated with deposits buried or outcropping at lower altitudes in the hanging wall (Blumetti et al., 2013; Calamita et al., 2000; Falcucci et al., 2015; Galadini & Galli, 2000; Galadini et al., 1998; Galli et al., 2015; Gori et al., 2007; Gori et al., 2011; Patruno & Scisciani, 2021; Pizzi et al., 2002; Pizzi et al., 2010; Pucci et al., 2016; Pucci et al., 2019; Roberts et al., 2010). The total number of LONG data is 52.

4. Definition of long-term throw rates in the central Apennines

Inspecting the literature while searching for available data, we realized that two main issues are afflicting the long-term throw rate estimations in the central Apennines.

The first is the need for a standard probabilistic framework for estimating long-term throw rates from a single offset feature. Usually, authors have provided cumulative fault offsets ΔF since a fixed time from the present, which we refer to as Δt (Table S1). In detail, for the central Apennines, stated offsets ΔF at the trace of the investigated faults are reported as bounded by two measurements, as a best estimate or as a lower/upper limit. Stated ages Δt are described as the best estimate or bounded by two dates or as a lower limit. Suppose the offset and age uncertainties ($\sigma_{\Delta F}$ and $\sigma_{\Delta t}$, respectively) are unambiguously defined. In that case, the form of ΔF and Δt distributions are explicit, and this allows for a complete treatment of both in a probabilistic sense. However, we needed to make some assumptions about offset and age distributions when their uncertainties weren't reported explicitly. In the following subsections we describe how we determined the ΔF and Δt distributions and their general trends.

The second issue is related to the definition of the long-term fault offset rates. Commonly, slip rates have been estimated in the central Apennines by dividing the observed displacement of the faulted landform by its age, that is $\Delta F / \Delta t$. However, suppose, as expected, the shear stress around the fault is not equal in the starting and final instants of the investigated period. In that case, a more correct equation to recover the long-term throw rate is $L = \Delta D / \Delta t$ with the total far-field displacement ΔD defined as

$\Delta D = \Delta F + \Delta E$	(1)

where ΔE is the (positive or negative) offset variation of elastic origin needed to recover the shear stress on the fault to its starting value at Δt. In that case, neglecting ΔE could result in an "apparent slip rate" which can be remarkably different from the real long-term one regardless of the slip history in the investigated period. This distinction becomes less significant for older offset features, whose offset is accumulated over more seismic cycles (McCalpin, 2009), and it can be neglected only for a stably-slipping frictionless fault.

Commonly, ΔE is unknown and deeply problematic to estimate; thus, it is overlooked in slip rate estimates of the central Apennines, resulting in a potentially misleading value. In subsection 4.3 "Definition and estimation of the net elastic throw ΔE" we report how we handled this problem.

4.1 Single throw distributions in the central Apennines

In our dataset (Table S1), 287 data have a single "best estimate" throw ΔF. In 64 estimates, the stated throw is bounded by two limits; in 50 it is a lower (or minimum) limit, and in 2 cases it is an upper limit. These data usually refer to a vertical difference between two correlated peneplain remnants (Gori et al., 2007; Miccadei et al., 2002) or the displacement sum of two splays connected at depth (Galadini & Galli, 1999; Roberts & Michetti, 2004).

The uncertainty is directly reported in 55 measurements but can be indirectly deduced for 53 CHEA measurements, because the investigators furnished the standard deviation of the dip angle. We defined the standard deviation as one-half of the increment due to increasing (or decreasing) the rightmost significant digit by unity for data without quoted standard deviations. As an example, the inferred standard deviation of an offset measurement of 7.4 m is 0.05 m.

4.1.1 Stated offset is the best estimate

For the 287 offsets reported as best-estimates we assumed a Gaussian distribution. As there is no evidence of tectonic inversion during the Late Pleistocene/Holocene on the studied faults, it is appropriate to truncate (and renormalize) the Gaussian distributions so that they are limited to positive throws. That is, if we consider an offset f', given the measured offset ΔF_n and related standard deviation $\sigma_{\Delta F_n}$, its probability is given by:

$$p_{\Delta F}(f') = N\left(\begin{cases} 0; & f' < 0 \\ \dfrac{1}{\sigma_{\Delta F_n}\sqrt{2\pi}} \exp\left(\dfrac{-(f'-\Delta F_n)^2}{2\sigma_{\Delta F_n}^2}\right); & f' \geq 0 \end{cases}\right) \quad (2)$$

where $N(\ )$ is a dimensionless normalizing operator generically defined as

$$N(y(x)) \equiv \frac{y(x)}{\int_{-\infty}^{+\infty} y(x')\,\mathrm{d}x'} \quad (3)$$

4.1.2 Stated offset is bounded by two limits

For the 64 measurements with stated throw bounded by two limits, we assume that this range corresponds to the $3\sigma_{\Delta F_n}$ interval (87%-confidence interval) and that the mean of the two limits is ΔF_n. Both $\sigma_{\Delta F_n}$ and ΔF_n are then used in equation (2) to determine the distribution of ΔF (see Figure 2).

4.1.3 Stated offset is a lower limit

For 50 measured offsets the investigators warned that the actual throw is higher than the reported minimum $\Delta F_{\min}$. This occurs because the coseismically-displaced layer is found only in the hanging wall but not in the footwall, from which it has been eroded. In other cases, datable layers are suspended over the footwall but buried under an unknown thickness of younger deposits in the hanging wall (Galadini & Galli, 2000; Galli et al., 2015). In this case, we can define:

$$p_{\Delta F}(f') = N\left(\begin{cases} 0 & f' < 0 \\ p_{\Delta F}^{\text{prior}}(f')\dfrac{1}{2}\left[1+\operatorname{erf}\left(\dfrac{f'-\Delta F_{\min}}{\sqrt{2}\sigma_{\Delta F_{\min}}}\right)\right] & f' \geq 0 \end{cases}\right) \quad (4)$$

where the probability density function $p_{\Delta F}^{\text{prior}}$ is the prior estimate of long-term throw (during the measurement epoch) for the 59 faults and it is determined by bootstrap as explained in subsection 4.4 "Prior slip rates and bootstrap". See Figure 2 for the plot of the equation (4).

4.1.4 Stated offset is an upper limit

When the measured offset is defined as an upper limit $\Delta F_{\max}$, the probability density function for the offset f' is a boxcar smoothed around the upper limit

$$p_{\Delta F}(f') = N\left(\begin{cases} 0; & f' < 0 \\ \dfrac{1}{2\Delta F_{\max}}\operatorname{erfc}\left(\dfrac{f'-\Delta F_{\max}}{\sqrt{2}\cdot\sigma_{\Delta F_{\max}}}\right); & f' \geq 0 \end{cases}\right) \quad (5)$$

To this aim the complementary error function (erfc) is used (Figure 2).

4.2 Single age distributions

The investigators have reported the feature age Δt in different ways: 107 measurements are bounded by two dates, 293 are reported as the best-estimate and 3 as lower limit. If not explicitly reported, we consider $\sigma_{\Delta t}$ as one-half of the increment caused by increasing the rightmost significant digit by unity.

4.2.1 Two dates bound stated age

Many offsets have age constrained by dated stratigraphic successions. For example, the age of earthquakes in paleoseismological trenches is often bounded by the youngest dislocated deposits (age $\Delta t_{\min}$) and the oldest sealing/overlap sedimentary units (age $\Delta t_{\max}$). Similarly, for long-term estimates, Δt is bounded by two ages obtained by radiocarbon dating of collected samples (e.g., shells, charcoal, paleosoils) from two sedimentary or tephra layers. In these cases, the probability density function of age

t' to represent the starting time of the observed features is expressed by a smoothed-boxcar function given as:

$$p_{\Delta t}(t') = N\left(\begin{cases} 0; & t' \le 0 \\ \dfrac{1}{\Delta t_{\max} - \Delta t_{\min}} \dfrac{1}{2}\left[1 + erf\left(\dfrac{t' - \Delta t_{\min}}{\sqrt{2}\sigma_{\Delta t_{\min}}}\right)\right] \dfrac{1}{2} erfc\left(\dfrac{t' - \Delta t_{\max}}{\sqrt{2}\sigma_{\Delta t_{\max}}}\right); & t' > 0 \end{cases}\right) \quad (6)$$

4.2.2 Stated age is the best-estimate

In the vast majority of best-estimates, their value is dictated by the regional determination of the ice retreat following the Last Glacial Maximum, generally reported to occur 15±3 kyr BP. However, we noted that different authors refer to the same major climate change (the end of the Last Glacial Maximum), reporting different values and standard deviations, thus assuming different distributions. Note that the age of these features is often not experimentally determined but just assumed by field investigators. These are the common drawbacks of secondary sources summarizing the previous literature in the region without performing any new (primary) investigation. In a statistical study of western US fault-offset database (Bird, 2007), the error rate of such secondary sources was shown to be about three times that of primary literature sources. However, we do not want to risk contaminating our study by inserting these diverse climate models; therefore, we homogenized the Δt and $\sigma_{\Delta t}$ of Bubeck et al. (2015); Faure Walker et al. (2009); Faure Walker et al. (2019); Morewood and Roberts (2000); Papanikolaou et al. (2005); Roberts and Michetti (2004); Wilkinson et al. (2015) to the values suggested by Faure Walker et al. (2010) (15±3 kyr BP), defining the following probability density function of age t' (see Figure 2 for its plot)

$$p_{\Delta t}(t') = N\left(\begin{cases} 0; & t' < 0 \\ \dfrac{1}{\sigma_{\Delta t}\sqrt{2\pi}} \exp\left(\dfrac{-\left(t' - \Delta t_n\right)^2}{2\sigma_{\Delta t}^2}\right); & t' \ge 0 \end{cases}\right) \quad (7)$$

4.2.3 Stated age is a lower limit

Galadini and Galli (2000), relying on a series of stratigraphical considerations, determined a throw of 200-340 m for a truncated valley placed at the footwall of the Campo Felice fault. The truncation onset predates the till deposition (age 0.25 Myr) and postdates the inception of the central Apennines extension (1 Myr). In two other cases (F0011NLGMA08 and F0036NTRCH04) the reported Holocene throws predate a fixed age, but for these estimates, it seems unrealistic that they formed since the inception of the extension. To avoid any artifacts resulting in implausibly low rates, we assumed that any stated minimum age Δt_{min} also provides an order-of-magnitude estimation of the maximum age ($\approx 10 \cdot \Delta t_{\min}$) defining probability density function of age t' as

$$p_{\Delta t}(t') = N\left(\begin{cases} 0; & t' \le 0 \\ \frac{1}{2}\left[1+\operatorname{erf}\left(\frac{t'-\Delta t_{\min}}{\sqrt{2}\cdot\sigma_{\Delta t_{\min}}}\right)\right]\lambda \inf\begin{cases}\exp\left[-\lambda\left(t'-\Delta t_{\min}\right)\right] \\ 1\end{cases}\frac{1}{2}\operatorname{erfc}\left(\frac{t'-\Delta t_{\max}}{\sqrt{2}\cdot\sigma_{\Delta t_{\max}}}\right); & t' > 0 \end{cases}\right) \quad (8)$$

with $\lambda = -\ln(1/2)/\Delta t_{\min}$ (see Figure 2).

4.3 Definition and estimation of the net elastic throw ΔE

Styron (2019) showed that slip rate estimates calculated over time intervals shorter than the joint duration of ten earthquakes (causing slip at the sampled point on the fault trace) have the highest chances of being inaccurate if they use only Δt and ΔF. This issue can be managed (by increasing uncertainties appropriately) if we consider (and add) an equivalent fault offset ΔE needed for recovering the fault shear stress conditions at Δt. However, the exact value of shear stress at Δt for any offset feature is unknown and we can proceed only in a probabilistic way. We can speculate that under the assumption of a quasi-periodic behavior of the studied fault, its shear stress is rather low after each earthquake. Differently, if clustered earthquake recurrence is assumed, the potential for some greater elastic offsets must be considered. One complex way to approach this issue would be to develop a model investigating the variation of the elastic strain in a long-time (several million years) fault history, then sampling its ΔE changes across time windows of varying lengths, with many randomly selected starting times. Then, we would use empirical functions to describe how the probability density functions of the modeled ΔE varies with the time-window length and with the other parameters of the simulation, such as long-term fault rate and coefficient of variation, COV. This lengthy process would necessarily be based on a selective choice of input parameters. However, no definitive evidence for a clustered recurrence interval, and no data to score the model are available. In this differentiation, we follow Styron (2019) in defining the periodic distribution as one of the earthquakes occurring more regularly than randomly. Statistically, a fault with a periodic distribution of the seismicity has its $\mathrm{COV} = \sigma_{RI}/\mu_{RI} < 1$, where μ_{RI} is the mean recurrence interval and σ_{RI} is the standard deviation of the recurrence intervals. Instead, a clustered distribution of the fault seismicity ($\mathrm{COV} = \sigma_{RI}/\mu_{RI} > 1$) implies the occurrence of both tightly-spaced and widely-separated earthquakes.

Different authors have no consensus on the earthquake recurrence interval in the central Apennines, though the majority described quasi-periodic earthquake recurrences for various faults (Galli, 2020; Galli et al., 2008). As an example, Galli (2020) recently reports an exhaustive review of paleoseismological data showing a well-defined quasi-periodic earthquake recurrence. Conversely, slip histories found by Schlagenhauf et al. (2011) and Benedetti et al. (2013) suggest that the observed displacement is not periodic. Notably, in these works, the amount of coseismic slip is not related to the duration of the previous interseismic interval. Hence, we decided to determine ΔE independently for each offset feature, assuming that it should have a distribution resembling the one observed in the past coseismic

throws in the central Apennines, which sometimes represents a single event but sometimes represents the total throw in an earthquake doublet or larger cluster. With this assumption, the determination of ΔE is closer to the quasi-periodic distribution of seismicity, but not excluding some influence from the clustered one.

To this end, we collected all single-earthquake throws determined with CHEA and TRCH methods. The resulting paleoearthquake throw dataset is provided in Table S2, and it consists of 150 measurements (69 determined with CHEA and 81 with TRCH). Investigators supplied all the needed information to rely on equations (2)-(5) so we treat throw distributions in a probabilistic sense. Thus, we merged the 150 distributions, and the resulting PDF and CDF are shown in Figure 3. It can be noted that the two sub-datasets differ substantially with CHEA method detecting bigger throws than TRCH. As CHEA investigators usually sample steep slopes, we suspect that some gravitational mass-wasting effects could amplify the coseismic signal locally, as recently pointed out by Di Naccio et al. (2019). In any case, this marked difference in the final PDFs and CDFs is expected to capture both the stochastic variability of coseismic throws and the potential for some greater elastic throws. In the last step, we fitted the normalized CDF throw distribution with the exponential curve:

$P(C \le c) \cong 1 - \exp(-\lambda c)$	(9)

where c is the coseismic throw in a single earthquake. We found $\lambda = 1.0$ m^{-1}, implying that c_m the mean paleoseismic throw ($c_m = 1/\lambda$) for the central Apennines faults is 1 m. Its standard deviation ($\sqrt{1/\lambda^2}$) is 1 m, too.

The development of equations for estimating the probability density function of ΔE (to recover the fault shear stress level at Δt) for different measuring times follows Bird (2007). For young offset features (small Δt), the model distribution of ΔE is asymmetric, with a small chance of a large negative change (due to an earthquake, modeled using the distribution of c'), and a larger chance of net elastic strain accumulation without an earthquake (modeled with the current bootstrap estimate of the fault throw rate). For old offset features with Δt greater than typical earthquake recurrence times (1-3 kyr), the distribution of ΔE will be based on mirroring the distribution of c' about zero, and halving it. That is, the chances of net positive and net negative changes in elastic strain become equal, and the magnitude is limited by the distribution of throws in one earthquake cluster, c'. It is necessary to create a smooth transition between these two end-member cases to contemplate all possible cases.

We proceeded as follows: given a positive strain ($e > 0$), the probability of an even greater elastic offset ($e < \Delta E$) can be expressed as the product of two factors. The first factor is the probability that e is loaded

in Δt according to the prior distribution of long-term offset rates. The second term is the probability that ℓ could be released in a single pseudo-earthquake according to the exponential curve determined above. That is:

$$1-P\left(\Delta E \le e \,|\, \Delta E > 0\right) = P\left(e < L^{\text{prior}}\Delta t\right)P\left(e < C\right) \quad (10)$$

which becomes in terms of probability density function:

$$p_{\Delta E}\left(e'\right) \equiv -P\left(e' < L^{\text{prior}}\Delta t\right)\frac{\mathrm{d}}{\mathrm{d}e'}P\left(e' < C\right) - P\left(e' < C\right)\frac{\mathrm{d}}{\mathrm{d}e'}P\left(e' < L^{\text{prior}}\Delta t\right) \quad (11)$$

With its complete form being:

$$z\left(e'\right) = \exp\left(-\lambda e'\right)\left[\lambda\int_{e'}^{\infty}\int_{0}^{\infty} p_L^{\text{prior}}\left(\ell'\right)p_{\Delta t}\left(t' = \frac{e''}{\ell'}\right)\frac{1}{\ell'}\mathrm{d}\ell'\mathrm{d}e'' + \int_{0}^{\infty} p_L^{\text{prior}}\left(\ell'\right)p_{\Delta t}\left(t' = \frac{e'}{\ell'}\right)\frac{1}{\ell'}\mathrm{d}\ell'\right] \quad \text{for} \quad e' > 0 \quad (12)$$

as the expectation of $p_{\Delta E}$ is zero, the possibility of a negative offset is weighted with the factor k and jointly normalized in a way that there is an equal chance of having a gain or a loss in elastic offset:

$$p_{\Delta E}\left(e'\right) \cong N\left(\begin{cases} kp_c\left(c' = -e'\right) & e' \le 0 \\ z\left(e'\right) & e' > 0 \end{cases}\right) \quad (13)$$

We performed some exploratory tests and determined that any reported offset younger than 2 ka is likely to be strongly affected by such elastic offset (Figure S1) for the studied faults. In our method, for offset age <2 ka, the missing or excess elastic offset is mainly dependent on the assumed recurrence interval distribution, which in turn can be largely discordant with the real one of the single fault. Thus, we opted for the conservative choice of discarding any measured offset younger than 2 ka (Table S1). Similarly, we argue that throw rate variations based on offset features younger than 2 ka are probably dominated by short-term elastic behavior, thus likely to be not consistent.

4.4 Prior throw rates and bootstrap

In two cases (discussed above) we had to deal with incomplete information: a) when only a lower limit on the throw is available, $p_{\Delta F}^{\text{prior}}$ is required (see equation 4); b) when we need to estimate the probability that a missing or exceeding offset e' is higher than the measured throw (see equation 12), according to the prior distribution p_L^{prior}. In both cases, we can use the available measurements of all faults to estimate the corresponding p_L^{prior}. To this aim, we performed a two-step bootstrap estimation. In the first run, uniform "boxcar" distribution ($0 < L^{prior} \le 1.5$ mm/a) was set as model of the prior throw-rate probability density function for each single fault. After we computed all data-based $p_L\left(\ell'\right)$, they were averaged into one posterior throw-rate distribution, in which we have excluded the unbounded

rates, where the stated offset is a lower limit. In the second step, the posterior distribution was used as the prior one. After three iterations, the posterior distribution was almost entirely coincident with the prior one and we considered the datum-based prior distribution p_L^{prior} well-converged. Then, assuming $\Delta E = 0$, we can calculate $p_{\Delta F}^{\text{prior}}(f')$, the prior distribution for the long-term fault throw

$$p_{\Delta F}^{\text{prior}}(f') = \int_{-\infty}^{\infty} p_L^{\text{prior}}(\ell')\, p_{\Delta t}(t' = \frac{f'}{\ell'})\frac{1}{\ell'}\mathrm{d}\ell' \quad (14)$$

and use it in equation 4 (where only a lower limit is available) to determine the distribution of throw $p_{\Delta F}(f')$.

4.5 Long-term offset rate L for a single measurement

Once $p_{\Delta F}$ and $p_{\Delta E}$ have been determined, we convolve them to calculate the probability density function of the far field long-term offset defined as

$$p_{\Delta D}(d') = N\left(\begin{cases} 0 & d' \le 0 \\ \int_0^{+\infty} p_{\Delta E}(e')\, p_{\Delta F}(f' = d' - e')\mathrm{d}e' & d' > 0 \end{cases}\right) \quad (15)$$

and finally, we can determine the probability density function of the long-term throw rate p_L for each reported measurement as

$$p_L(\ell') = \int_0^{+\infty} p_{\Delta t}(t')\, p_{\Delta D}(d' = \ell' t')t'\mathrm{d}t' \quad (16)$$

This equation allows defining the probability of value ℓ' to be the long-term throw rate based on a single offset feature.

5. Pattern of long-term throw rates across the central Apennines

After inspecting the available literature for active normal faults in the central Apennines, we collected 403 different throw measurements performed with four different techniques (Table S1 and Figure 1), which are plot against reported age for each single fault in the Figure S2. Numerical-modeling methods applied to ^{36}Cl-cosmogenic radionuclide and earth trace elements concentrations in footwall carbonates (CHEA) allowed the dating of 73 throws. Last post-glacial (12-20 kyr) geomorphic markers and deposits recognition (LGMA) resulted in 232 data reporting the vertical separation of originally subplanar or sublinear features. Field mapping of dislocated Middle-Late Pleistocene stratigraphic layers/geomorphic features (LONG technique) resulted in 52 offset rates. Paleoseismic trenching studies (TRCH) constrained 46 offsets and related ages.

A closer inspection of the sampled ages reveals that the most-investigated time interval of central Apennines fault evolution is the past 25 kyr, and the most sampled time interval being the $\Delta t \approx 15$ kyr (Figure 4). This peak is due to a large number of LGMA measurements. A second peak is found at ~3-5 kyr, roughly corresponding with the most abundant estimates of TRCH and CHEA techniques.

We found that the median of all fault throw rate estimates is 0.5 mm/yr, with a 90%-confidence range of 0.08-1.48 mm/yr (Figure 5). However, this is the only phase of our study in which rates from different normal faults are combined; in the following phases, we consider and model only rates measured along one fault.

Subdividing the rates by measurement technique (but still lumping all faults together), the 90%-confidence range for LONG constrained throw rate is 0.06-1.16 mm/yr (median 0.42 mm/yr). The general pattern of TRCH throw rates (90%-confidence range 0.04-1.54 mm/yr, median 0.36 mm/yr) is similar to the LONG ones, with the main difference resting in higher probabilities for fast rates. This discrepancy occurs because the offsets in normal faults are often reported as a lower limit, potentially allowing higher values, whereas the age of deformed Middle-Pleistocene units or features is usually well constrained. The confidence range is 0.10-1.40 mm/yr (median 0.50 mm/yr) for LGMA estimates, instead, the 90%-confidence range limit for CHEA is 0.14-1.74 mm/yr with median 0.68 mm/yr (Figure 5). The throw rates determined for each fault are plotted against age in Figure S3.

The cumulative distribution of the throw rates in the central Apennines can fit a lognormal distribution with a mean of 0.63 mm/yr and a standard deviation of 0.55 mm/yr (red line in Figure 5).

5.1 Treatment of uncertainties for ΔF and Δt

The uncertainty quantification for both ΔF and Δt is different among techniques and authors. Often a simple experimental uncertainty (observation error) is provided whereas in few cases additional epistemic uncertainty is discussed. However, a homogeneous treatment of uncertainties is required for a coeherent data comparison. Following the popular distinction between “aleatory” and “epistemic” uncertainties, we can assume that they are uncorrelated for all throw measurements of the central Apennines and that the “aleatory” uncertainties are mainly defined by the “observational” uncertainties in our paper. Thus the total uncertainty for each measurement would be defined from the Pythagorean sum of both aleatory and epistemic uncertainties.

We inspected how the observational uncertainties vary in time for all features of our database by plotting ΔF and Δt 95% Confidence Levels (95% C.L.). We limited our analyses to $\Delta t < 25$ kyr, as most fault throw rates were collected in this time interval (Figure 4).

Both confidence intervals expand in time, though the increase is more evident for Δt. With the notable exception of LGMA measurements, $\sigma_{\Delta t}$ was provided by laboratory analyses. The expertise of field

investigators may be adequate to avoid or limit any other age uncertainty source, also considering the relatively small Δt. Thus, the observation error reasonably corresponds to the total uncertainty ($\sigma'_{\Delta t} = \sigma_{\Delta t}$), and it is almost 15% of Δt itself (Figure 6). We recall that for many LGMA measurements, we homogenized the Δt uncertainties to the values suggested by Faure Walker et al. (2010). Note that the age of these features is often not experimentally determined but just assumed by regional features correlation. This assumption may be a severe limitation for using these data because it could become a tight constraint on the resulting offset rate when paired with a too-narrow definition of $\sigma_{\Delta t}$. However, we consider the reported $\sigma_{\Delta t} = 3$ kyr a sufficiently large uncertainty to further use these data for long-term estimates.

The 95% C.L. of ΔF is less pronounced and more variable than the Δt one and can be approximately fit with a linear increase with age of the feature. The smaller increase as age function of ΔF uncertainties to Δt ones is not surprising because the investigators often report only the observation errors. In this case, it is questionable to assume that epistemic uncertainties are negligible. For example, in LGMA measurements, ΔF is often provided with the precision of a metric ruler. Still, exhaustive discussion and quantification of other uncertainty sources define much greater values (as an example, see Papanikolaou et al., 2005). We will show in section 6 how influential is a correct estimation of the total uncertainty in long-term estimates.

6. Determining fault throw rate variance

6.1 Noisy throw rate profiles

The throw and throw-rate profiles measured along several active faults taper out with characteristic gradients towards the fault tips. Different slip (and slip-rate) profiles collected in several tectonic environments seem to be related to the fault dynamics. Inelastic deformation governs linear slip gradients near the tips, and elliptical shapes describe purely elastic slip distributions (Scholz & Lawler, 2004). We plotted the throw-rate profiles for some faults sampled with at least ten measurements points and three different techniques to capture a typical profile for the central Apennines active faults. We followed Manighetti et al. (2001), normalizing the distance to the fault length and the throw-rate to the highest median value among the data of each fault (Figure 7 and Figure S4).

The visual inspection of along-strike throw-rate profiles clearly shows a high scattering among data, which does not define any clear throw-rate shape. This overdispersion requires a better investigation of both uncertainty sources and data contamination before assigning any specific rheological meaning to the observed throw rate profiles.

6.2 Throw rate disagreement curves for the central Apennines

Regardless of the slip gradients near unconnected fault tips or the fault history, two features close in time and space and sampling the same fault activity are expected to provide comparable long-term estimates. Contrarily, more distant (in space or in time) features are expected to sample more different rates. This contrast between close and distant data pairs should appear in some form when inspecting the dataset of active faults if throw rates are uncontaminated by noise. This step is fundamental to discriminate spatial and temporal variabilities from throw rate variance. The former is a tectonic signal and the latter is noise to be addressed by further modeling, as an example in PSHA. We can distinguish these two-end members if a clear definition of disagreement among throw rate estimates of the same fault is available.

Because the long tails of most individual throw rate distributions (PDFs) at single sites are potentially overlapping to some extent, we opted for a probabilistic definition of disagreement to a purely binary classification. Let us consider two throw-rate probability distributions of two independent measurements A and B. If we define a value x (Movie S1), a sufficient condition for the two independent measurements to be different is that A and B are always separated by x. Thus we can use the scalar quantity δ:

$$\delta \equiv \sup_{x=0}^{\infty}\left\{P(A<x\le B)+P(B<x\le A)\right\} \qquad (17)$$

which becomes in our case

$$\delta \equiv \sup_{x=0}^{\infty}\left\{P_L^A(A<x)\left[1-P_L^B(B<x)\right]+P_L^B(B<x)\left[1-P_L^A(A<x)\right]\right\}= \sup_{x=0}^{\infty}\left\{P_L^A(A<x)-2P_L^A(A<x)P_L^B(B<x)+P_L^B(B<x)\right\} \qquad (18)$$

The possible values of disagreement δ span between 0.5 and 1. If the median of the two distributions is coincident, then $\delta = 0.5$ regardless of the stated standard deviations. However, if the two distributions are completely discordant without any overlapping interval, then $\delta = 1$ (Movie S2).

Calculating the disagreement δ makes sense only if we consider data pairs sampling the rate of the same fault. To this aim, we assigned each throw rate to its fault and determined the disagreement δ of it to all other throw rates collected along the same fault. This operation resulted in 3466 data pairs for the 59 fault traces. As we are interested in the overall trends of our dataset, we merged and sorted the 3466 disagreements building the cumulative distribution of disagreements shown in Figure 8. Furthermore, we split the disagreement dataset into several subsets to inspect the variance among different methods in sampling the fault throw rates. The resulting curves are also plotted in Figure 8, where we also report along the distribution curve the value β describing the fraction of highly-disagreeing data pairs ($\delta \ge 0.95$)

It can be noted in Figure 8 that β is never the highest for data collected with the same method. The only exception is LONG measurements ($\beta = 0.28$), which examine larger time intervals and likely sample actual long-term variations. However, their scarce number, along any studied fault, doesn't allow investigating this conjecture in greater detail. The worst pairing for the remaining methods is between data pairs comparing LGMA measurements ($\beta = 0.16$). Also for CHEA and TRCH the worst pairing is with LGMA ones ($\beta = 0.11$ for CHEA-LGMA; and $\beta = 0.07$ for TRCH-LGMA). This increase of β when pairing different methods implies that the variability in throw rates is most apparent when the fault has been investigated with alternative techniques.

To discriminate the noise from signal, we sorted the 3466 disagreements according to spatial separation of the data pair. We also sorted the δ dataset by time-span between the ages of the two offset features in each data pair. If spatial separation were important, then disagreements between data should increase systematically with distance, regardless of the specific fault kinematic model. Likewise, if time-separation were important, then disagreements between data should increase systematically with the difference in ages of the offset features, regardless of the specific time-history proposed. Figure 9 shows the graphical analysis of β (fraction of high disagreement data) versus age-differences and relative along-fault positions between all possible data pairs sampling the throw rate for the same fault. These graphs do not support either space or time as critical independent variables. Instead, they seem to suggest a high degree of randomness as a distinctive characteristic of the dataset, as already shown by the throw-rate profiles along certain well-studied fault traces (Figure 7). These spatial and temporal patterns also seem to be confirmed at the single-fault scale (Figure S3 and Figure S4). Furthermore, the slight reduction in disagreements for separations under 1 km probably results from the increased likelihood that such pairs used the same measurement technique and even came from the same published study.

6.3 Determination of ΔF epistemic uncertainties ($\sigma'_{\Delta F}$) with throw rate forward modeling and disagreement curve comparison

The disagreement curves recovered for the central Apennines have strong implications for throw rates estimates and uncertainty quantification. In general, when the disagreement of a data pair approaches one ($\delta \geq 0.95$), three alternatives become equally valid and mutually exclusive: a) both data are erratic (non-tectonic) measurements; b) the data pair is formed from one correct datum and one erratic one; c) the two values are correct and the high disagreement comes from the measurement uncertainties. Considering that β is the percentage of pairs with $\delta \geq 0.95$ in our real dataset, these three alternative possibilities can be merged and used to determine the fraction of incorrect data α solving the equation:

$\beta = \alpha \cdot \alpha + (1-\alpha) \cdot \alpha + \alpha \cdot (1-\alpha) + \gamma \cdot (1-\alpha) \cdot (1-\alpha)$	(19)

where γ represents the possibility that $\delta \geq 0.95$ results from sampling the tails of two correct data pair distributions.

For the disagreement curve of real data, we have determined $\beta = 0.13$ (Figure 8). If we assume that field investigators were able to detect tectonic features and distinguish them from non-tectonic, then we would expect $\alpha \approx 0$ and $\beta \approx \gamma$ in equation (19). Differently, for $\beta > \gamma$ and $\alpha > 0$ we have to suppose that field investigators misinterpreted some non-tectonic features as tectonic ones. Thus, the calculation of γ is crucial for discriminating between these two alternatives.

To this end, we need to build different datasets characterized by the same uncertainties in both ΔF and Δt measurements. In section 5, we have found that the 95% C.L. of both ΔF and Δt can be modeled by linear functions of age of the offset feature. Assuming that the 95% C.L. roughly corresponds to 4σ (as it does in a normal distribution), we can assume that for each datum (real or synthetic) the observational $\sigma_{\Delta F}$ can be replaced with $\sigma'_{\Delta F}$ having the value of $\sigma'_{\Delta F} = \Delta\tilde{t} \cdot 0.05$ mm/yr where $\Delta\tilde{t}$ represents the median of the Δt distribution. Instead, the observational age uncertainty is set to $\sigma'_{\Delta t} = \Delta\tilde{t} \cdot 0.15$.

In a first model we assumed $\sigma'_{\Delta t}$ and $\sigma'_{\Delta F}$ to coincide with the nominal observational (aleatory) uncertainties and we used the ΔF and Δt measurements as in Table S1. In Figure 10 we show the similarity of this modeled disagreement curve (black line in Figure 10A) to the real one (dotted red line in Figure 10A). These similar trends suggest that the linear functions to the feature age are good proxy of observational uncertainties. This allows performing a synthetic test to determine γ from the theoretical distribution curves of disagreements between any purely tectonic offset rates.

To this end, we created 135 slip (throw) histories using the observed throw rates and coseismic throws (Table S1 and Table S2). In detail, the cumulative distributions indicate that the throw rate dataset describes the activity of a series of active faults with 0.63 mm/yr (and standard deviation 0.55 mm/yr, Figure 5) long-term throw rate and 1 m (standard deviation 1 m) mean earthquake displacement (Figure 3). Considering the uncertainties on both the throw rate and throw distributions, we assumed a return period of 1600 ± 1600 yr for each of the 135 modeled fault histories.

We sampled ten times each fault history in the 2-25 kyr time interval, which contains 87% of the observed throw rate measurements. Then we perturbed each age and throw with a Gaussian noise of $\sigma'_{\Delta t} = \Delta\tilde{t} \cdot 0.15$ and $\sigma'_{\Delta F} = \Delta\tilde{t} \cdot 0.05$ mm/yr. Finally, we randomly selected Δt and ΔF in the perturbed distribution intervals and built a synthetic feature dataset. We meta-analyzed this synthetic dataset in the same way as the real one to determine the Δt, ΔF and ΔE distribution curves of each synthetic measurement and then its long-term throw rate distribution L. This synthetic dataset contains ideal tectonic measurements perturbed only by observation errors. Thus, we determined the disagreement

curve for this ideal dataset as done for real data and shown in Figure 8, by comparing the long-term throw rates of each data pair sampling the same active fault. From the resulting disagreement curve, shown in Figure 10A, we determined γ=0.03.

Recalling equation 19 and the fraction of high disagreeing data observed in our dataset (β=0.13), then considering γ=0.03, we obtain α≈0.05. This result implies two different scenarios: if we assume that the observation uncertainties ($\sigma_{\Delta t}$ and $\sigma_{\Delta F}$) coincide with the total ones ($\sigma'_{\Delta t}$ and $\sigma'_{\Delta F}$), then several data (5%) sampled non-tectonic features along the fault traces. Alternatively, if we maintain that field investigators have the expertise to detect tectonic features and distinguish them from non-tectonic ones, then the ΔF total (observational and epistemic) uncertainties ($\sigma'_{\Delta F}$) are higher than the observational errors $\sigma_{\Delta F}$. We opted for this latter alternative.

We focused on $\sigma'_{\Delta F}$ because the short length of the investigation period (<25 kyr), the steady-state of long-term geodynamic settings for the central Apennines, and the laboratory uncertainties suggest that total and observation uncertainties may not differ significantly for the age of observed features thus we set always $\sigma'_{\Delta t} \approx 0.15 \cdot \Delta t$. Then, we tested different values of $\sigma'_{\Delta F}$, used it to determine the Δt, ΔF and ΔE distribution curves of each datum and then the long-term throw rate distributions L. We built the disagreement curve and compared it to the synthetic one searching for the $\sigma'_{\Delta F}$ value minimizing the difference between β and γ of two curves. Finally, we found that $\beta \square \gamma$ (α≈0) for $\sigma'_{\Delta F} = \Delta\tilde{t} \cdot 0.10$ mm/yr (Figure 10C). In Figure 6 we have plotted all tested $\sigma'_{\Delta F}$ and in red the optimal value $\sigma'_{\Delta F} = \Delta\tilde{t} \cdot 0.10$ mm/yr. It can be observed in Figure 6 that this total uncertainty doubles or triples the observational one ($\sigma_{\Delta F}$) of LGMA estimates, which are largely predominant in for 10 kyr < Δt < 20 kyr. For graphical inspection, we report single throw rate estimates L for both nominal (observational) and total ($\sigma'_{\Delta F} = \Delta\tilde{t} \cdot 0.10$ mm/yr) uncertainties in Figure S5.

7. Fault long-term throw rates

The meta-analyses performed on our throw rate dataset suggest that it is affected by noise contamination causing overdispersion with respect to the computed resultants of nominal observational uncertainties. For this reason, we propose a base model (null hypothesis) of uniform throw rate along each fault trace (except tapering to zero at unconnected ends). Also, we consider that temporal variations in throw-rate remain unproven, and may constitute over-fitting. To this aim, we recalculated the prior throw rate distribution p_L^{prior} and the single-measurement throw rate distributions $p_L(\ell')$

using the new age-dependent epistemic uncertainty $\sigma'_{\Delta F}$ for each datum. Then, we determined the fault long-term throw rates combining all the measurements I of each fault as

$$\left\{p_L^{combined}\left(\ell'\right)\right\}^i \cong N\left[\left\{p_L^{combined}\left(\ell'\right)\right\}^{(i-1)}\left\{p_L^i\left(\ell'\right)\right\}\right] \quad (20)$$

for all i in the range $1 \le i < I$ with $\left\{p_L^{combined}\left(\ell'\right)\right\}^0 = 1$. The 95% C.L. and the median values of the probability density function of the combined throw rate $p_L^{combined}$ are reported in Table 1 and shown in Figure S6. Median values are plotted on map in Figure 11.

The most prominent spatial pattern of the resulting estimates is the almost-uniform throw rate for the faults in the central sector of the chain, which roughly corresponds with the area characterized by the highest geodetic strain rates (Carafa et al., 2020).

The fastest slipping faults (> 0.97 mm/yr) are Liri, Fiamignano, Barisciano-San Pio delle Camere and Assergi. These faults are not adjacent and are located in different sectors of the chain. Given that the maximum extension of the central Apennines migrated eastward since Pliocene (Calamita & Pizzi, 1994; Piacentini & Miccadei, 2014), the distribution of these fast-slipping faults could be linked to the geodynamic evolution of the chain. However, this hypothesis is weak because these fast-slipping faults are close to other slow-to-intermediate slipping ones.

For assessing the relative precision of each estimate, we defined the coefficient of variation (COV) as the ratio of the 95% confidence interval to the median of the throw rate distribution (Figure 11). COV values lower than one intuitively suggest a pretty well-defined throw rate in the number of measurements and their compatibility. However, COV values close or above one characterize scarce and/or mostly scattered offset features, as the Assergi fault. Figure 11 shows that the north-western and easternmost active faults are less investigated, and more effort is needed to narrow the uncertainty on their activity rates.

8. Discussion

We applied a meta-analysis to dated throw features on the active normal faults of the central Apennines, and determined their long-term throw rates. We found a large overdispersion of rates with respect to nominal observational uncertainties which implies that total uncertainties are two to three times bigger than the stated observational uncertainties. These results agree with the findings of McPhillips and Scharer (2018) and indicate that natural (but non-tectonic) or anthropogenic landscape modifications justify the augmentation of the observational errors by epistemic errors when computing long-term throw rate estimates. Here we discuss some possible causes.

8.1 Method-related noise

We have shown that variations in fault throw rate are apparent when inspecting data collected with different techniques applied to the same fault, and any method-specific systematic bias is revealed by comparing measurements taken with alternative methods. For example, in ^{36}Cl dating, the sampling bias favors slip estimates fitting the bottom of the fault scarp, the portion with higher data density (Goodall et al., 2021). This method limitation can be unveiled only by comparing different techniques and their individual assumptions.

Different strategies for selecting the measurement sites along the same fault seem to further increase the probability of sampling slip rate randomness or non-tectonic effects. Thus, it is not surprising that well-trained investigators contested the alleged tectonic source of some previously reported offset features. Goodall et al. (2021) supposed that some fast throw rates on the Middle Aterno Valley fault (F0015NCHEA01, F0015NCHEA02, and F0015NCHEA03 offset measurements in Table S1) are due to net erosive slope processes that likely removed material from the hangingwall slope resulting in a higher scarp. Kastelic et al. (2017) proved an equivalent non-tectonic short-term exposure rate for several faults in the central Apennines and some measurement points along the Campo Felice fault scarp investigated by Goodall et al. (2021).

Another severe method-related limitation is the minimum sampled age. Using a bootstrap strategy to estimate the size of shear stress variations around a typical fault during its simulated earthquake history, we showed that offset features younger than 2 ka must be considered to give only an “apparent tectonic rate”. This estimate may be quite different from the long-term one, because the state of shear stress surrounding the fault may have changed, and this effect is material for small/young offsets (Figure S1). For these estimates, some increase in the throw uncertainty is needed before determining the long-term throw rates (which, by definition, would not include any short-term elastic-strain effects). This point confirms our findings on method-related variance not being marginal; it may have been overlooked by other investigators focused on proving spatial and temporal variability of fault slip rates.

8.2 Surface processes noise

In the coseismic phase, gravity and rheological variations are well-documented to amplify the tectonic signal at the ground surface (Chen et al., 2012; Di Naccio et al., 2019; Roback et al., 2018). That is, the height of a tectonic normal fault scarp may be amplified by incipient landslding and compaction in the hangingwall, especially when it is composed of incoherent talus. In these circumstances, even extensive field investigations can hardly distinguish non-tectonic from tectonic deformation in the near-surface due to the geomorphic convergence of the alternative or coexisting processes. Thus, it is likely that in some peculiar situations, the reported throw-rate feature is magnified (or reduced) by the effect of unrelated parameters or concurrent processes (Kastelic et al., 2017; Stemberk et al., 2019).

682 We suspect that such spurious amplifications of the tectonic signal are most likely at measurement sites
683 located on steep slopes. Some form of non-tectonic gravity-driven scarp growth is a significant
684 complicating factor in such settings, amplifying the tectonic signal. Previous analysis of coseismic offsets
685 measured after two main earthquakes that occurred in the central Apennines (Di Naccio et al., 2019)
686 have proved that above the critical slope angle of 30° slope failures may occur, and rock scarps are
687 expected to be amplified as a result. The extra accelerations and extra stresses due to seismic wave
688 passage can perturb the static equilibrium and cause the hanging wall to move short distances in short
689 times.

690 Also, the formation and evolution of the bedrock scarp may have been controlled by erosional
691 processes, which would act in the other direction, to reduce or hide the tectonic signal. This process has
692 been suggested by Galadini (1999) for the Liri fault (F0029N measurements in our dataset), which places
693 the highly-eroded Miocene flysch in contact with Mesozoic carbonate bedrock without tectonic
694 evidence for Late Pleistocene deposits. Furthermore, Papanikolaou et al. (2005) argued that, even if the
695 site selection was very careful, the fault scarp has inevitably been altered to some extent by weathering
696 and deposition, resulting in an underestimation of post-glacial throw.

697 ### 8.3 Future developments

698 Our meta-analysis shows that overdispersion is a distinctive data pattern in the central Apennines.
699 Consequently, we argue that the throw rate dataset cannot support any general and sophisticated fault-
700 growth model. For this reason, we attempted to calculate a model with the minimum number of
701 degrees of freedom needed for seismic hazard analysis: one uniform throw rate for each fault. Following
702 the “Occam’s razor” principle, the most defensible estimate would be only a uniform mean throw rate
703 with a clear definition of its uncertainty. And this is valuable because, up to now, no throw (or slip) rates
704 have been provided for the central Apennines that merged different estimates in a rigorous and
705 probabilistic framework, as we have.

706 Specifically, we are not contesting that fault throws and throw rates taper to zero at some unconnected
707 fault tips. Instead, (now) available data in the central Apennines do not allow defining the shape of this
708 tapering, which could be sharp at the tips or gentle and pervasive from the center of the fault. This
709 issue could be resolved in the central Apennines with a dramatic increase of measurements and
710 analyses on both coseismic throws and long-term throw rates. In this sense, our analyses support a
711 further increase in geological studies as recently done by Schirripa Spagnolo et al. (2021), paired with
712 deep seismic profiles (Buttinelli et al. 2021; Patruno & Scisciani 2021,) and geodetic data (Carafa et al.,
713 2020) for a better definition of single-fault throw rate, possibly varying in space and time.

714 Only three earthquake sequences in the past century (the 1915 Fucino earthquake sequence, the 2009
715 L'Aquila earthquake sequence, and the 2016-2017 Amatrice-Norcia seismic sequence) left continuous

and measurable marks. Thus, any long-term throw rate model based on fault trace estimates currently lacks enough data to be validated without any circular reasoning. Consequently, extreme caution (and complete definition of observational and epistemic uncertainties) is needed for seismic hazard modelers in using fault data.

Furthermore, we do not exclude that active faults could appear on the ground surface as arrays of en-echelon segments whose offsets are governed by laterally-variable rheology. In this context, non-characteristic and clustered earthquakes can amplify offset rate variability in space and time. Meta-analysis on the regional dataset using fault trace data alone cannot solve these issues due to data scarcity and noise contamination. Instead, lateral variability of fault activity can be better assessed if fault trace data are paired with mineralogical analyses on the composition of carbonate-hosted faults (Smeraglia et al., 2018; Smeraglia et al., 2017), because lateral variability of fault friction is expected to become evident. As in Doglioni et al. (2011) or Carafa and Barba (2011), patterns in fault rheology can then be included in rheological models to better predict and understand along-strike variability. Also, geochemical studies on fault-trace CO_2 degassing rate (Chiodini et al., 2020; Chodini et al., 2004) and the secular variation in geodetic time series can perhaps be related to the date of the most recent earthquakes (detected with paleoseismology and reported in Table S2) to discriminate whether faults exhibit any measurable time-dependent pattern(s).

9. Conclusions

We found that fluctuations in throw rates on active faults in the central Apennines are larger than the expected resultants of nominal observational errors. We also proved that their real tectonic significance remains highly questionable because these fluctuations are dominated by data overdispersion. If the apparent throw rate variability results from a long-term tectonic process, that would have crucial implications, justifying more complex time-dependent models in seismic hazard assessment. However, independent data (e.g., known climate or geodynamic changes) must parallel and thus confirm any apparent slip rate changes, which, otherwise, solely reflect both the inherited stochasticity of the earthquake processes and noise contamination.

Given the current understanding of temporal and spatial fault throw rate variability in the central Apennines and the epistemic uncertainties connected to the throw rate estimates, it is not yet feasible to produce more complex PSHA models. A base model with a uniform throw rate along the trace (tapering to zero at unconnected fault tips), and merging information from offset features of different ages to constrain a single time-independent rate, is still the most reasonable one.

Acknowledgments, Samples, and Data

Funding: The analysis described in this paper was carried out in the framework of the activities of INGV Seismic Hazard Center (Centro Pericolosità Sismica, CPS). This study has benefited from funding provided by the Italian Presidenza del Consiglio dei Ministri-Dipartimento della Protezione Civile (DPC). This paper does not necessarily represent DPC official opinion and policies.

Data Availability Statement

- All estimates have been obtained with a modified version of Slippery code (available at http://peterbird.name/oldFTP/Slippery/Slippery.f90.txt) adapted for the central Apennines kinematics and attached as Text S1.

- All data are cited and referenced in the text and are included in the following papers: Benedetti et al., 2013; Blumetti et al., 2013; Boncio et al., 2010; Bubeck et al. 2005; Calamita et al., 2000; Carcaillet et al. 2008; Cinti et al., 1992; Cinti et al., 2011; Cowie et al., 2017; D'Addezio et al., 2001; Falcucci et al., 2015; Faure Walker et al., 2009; Faure Walker et al., 2010; Faure Walker et al., 2019; Galadini and Galli, 1999; Galadini and Galli, 2000; Galadini et al., 1998; Galli et al. 2010; Galli et al. 2012; Galli et al. 2015; Giraudi and Frezzotti, 1995; Giraudi, 1988; Giraudi, 1989; Giraudi, 1995; Goodall et al., 2020; Gori et al. 2007; Gori et al., 2011; Gori et al., 2017; Manighetti et al. 2010; Miccadei et al., 2002; Morewood and Roberts, 2000; Moro et al., 2013; Pantosti et al, 1996; Papanikolaou et al., 2005; Patruno and Scisciani, 2021; Piccardi et al., 1999; Pizzi and Pugliese, 2004; Pizzi et al., 2002; Pizzi et al., 2010; Pucci et al., 2016; Pucci et al., 2019; Roberts and Michetti, 2004; Roberts et al., 2010; Salvi et al., 2003; Saroli et al., 2008; Schlagenhauf et al., 2009; Schlagenhauf et al., 2011; Tesson et al., 2016; Villani et al., 2015; Wilkinson et al., 2015.

References

Amos, C. B., Burbank, D. W., Nobes, D. C., & Read, S. A. L. (2007). Geomorphic constraints on listric thrust faulting: Implications for active deformation in the Mackenzie Basin, South Island, New Zealand. *Journal of Geophysical Research: Solid Earth, 112*(B3). https://doi.org/10.1029/2006JB004291.

Balco, G. (2011). Contributions and unrealized potential contributions of cosmogenic-nuclide exposure dating to glacier chronology, 1990–2010. *Quaternary Science Reviews, 30*(1), 3-27. https://doi.org/10.1016/j.quascirev.2010.11.003

Basili, R., Valensise, G., Vannoli, P., Burrato, P., Fracassi, U., Mariano, S., et al. (2008). The Database of Individual Seismogenic Sources (DISS), version 3: Summarizing 20 years of research on Italy's earthquake geology. *Tectonophysics, 453*(1), 20-43. https://doi.org/10.1016/j.tecto.2007.04.014.

Benedetti, L., Manighetti, I., Gaudemer, Y., Finkel, R., Malavieille, J., Pou, K., et al. (2013). Earthquake synchrony and clustering on Fucino faults (Central Italy) as revealed from in situ 36Cl exposure dating. *Journal of Geophysical Research: Solid Earth, 118*(9), 4948-4974, doi:10.1002/jgrb.50299.

Bird, P. (2007). Uncertainties in long-term geologic offset rates of faults: General principles illustrated with data from California and other western states. *Geosphere, 3*(6), 577-595. https://doi.org/10.1130/GES00127.1

Blumetti, A. M., Dramis, F., & Michetti, A. M. (1993). Fault-generated mountain fronts in the central apennines (Central Italy): Geomorphological features and seismotectonic implications. *Earth Surface Processes and Landforms, 18*(3), 203-223. https://doi.org/10.1002/esp.3290180304

Blumetti, A. M., & Guerrieri, L. (2007). Fault-generated mountain fronts and the identification of fault segments: implications for seismic hazard assessment. *Bollettino Societa Geologica Italiana, 126*(2), 307-322.

Blumetti, A. M., Guerrieri, L., & Vittori, E. (2013). The primary role of the Paganica-San Demetrio fault system in the seismic landscape of the Middle Aterno Valley basin (Central Apennines). *Quaternary International, 288*, 183-194. https://doi.org/10.1016/j.quaint.2012.04.040

Boncio, P., Lavecchia, G., & Pace, B. (2004). Defining a model of 3D seismogenic sources for Seismic Hazard Assessment applications: The case of central Apennines (Italy). *Journal of Seismology, 8*, 407-425.

Boncio, P., Pizzi, A., & Brozzetti, F. (2010). Coseismic ground deformation of the 6 April 2009 L'Aquila earthquake (central Italy, Mw6. 3). *Geophysical Research Letters, 37*, 2-7. https://doi.org/10.1029/2010GL042807

Bubeck, A., Wilkinson, M., Roberts, G. P., Cowie, P. A., McCaffrey, K. J. W., Phillips, R., & Sammonds, P. (2015). The tectonic geomorphology of bedrock scarps on active normal faults in the Italian Apennines mapped using combined ground penetrating radar and terrestrial laser scanning. *Geomorphology, 237*, 38-51.

Buttinelli, M., Petracchini, L., Maesano, F. E., D'Ambrogi, C., Scrocca, D., Marino, M., et al. (2021). The impact of structural complexity, fault segmentation, and reactivation on seismotectonics: Constraints from the upper crust of the 2016–2017 Central Italy seismic sequence area. *Tectonophysics*, 810, 228861. https://doi.org/10.1016/j.tecto.2021.228861

Calamita, F., Coltorti, M., Piccinini, D., Pierantoni, P. P., Pizzi, A., Ripepe, M., et al. (2000). Quaternary faults and seismicity in the Umbro-Marchean Apennines (Central Italy): evidence from the 1997 Colfiorito earthquake. *Journal of Geodynamics, 29*(3), 245-264. https://doi.org/10.1016/S0264-3707(99)00054-X

Calamita, F., & Pizzi, A. (1994). Recent and active extensional tectonics in the southern Umbro-Marchean Apennines (Central Apennines). *Mem. Soc. Geol. It, 48*, 541-548.

Carafa, M. M. C., & Barba, S. (2011). Determining rheology from deformation data: The case of central Italy. *Tectonics*, 30(2), doi:10.1029/2010TC002680.

Carafa, M. M. C., & Barba, S. (2013). The stress field in Europe: optimal orientations with confidence limits. *Geophysical Journal International*, 193(2), 531-548. https://doi.org/10.1093/gji/ggt024

Carafa, M. M. C., & Bird, P. (2016). Improving deformation models by discounting transient signals in geodetic data: 2. Geodetic data, stress directions, and long-term strain rates in Italy. *Journal of Geophysical Research: Solid Earth, 121*, 5557-5575, https://doi.org/10.1002/2016JB013038.

Carafa, M. M. C., Galvani, A., Di Naccio, D., Kastelic, V., Di Lorenzo, C., Miccolis, S., et al. (2020). Partitioning the ongoing extension of the central Apennines (Italy): fault slip rates and bulk deformation rates from geodetic and stress data. *Journal of Geophysical Research: Solid Earth* https://doi.org/10.1029/2019JB018956.

Carcaillet, J., Manighetti, I., Chauvel, C., Schlagenhauf, A., & Nicole, J.-M. (2008). Identifying past earthquakes on an active normal fault (Magnola, Italy) from the chemical analysis of its exhumed carbonate fault plane. *Earth and Planetary Science Letters, 271*(1), 145-158. https://doi.org/10.1016/j.epsl.2008.03.059

Cavinato, G. P., & Celles, P. G. D. (1999). Extensional basins in the tectonically bimodal central Apennines fold-thrust belt, Italy: Response to corner flow above a subducting slab in retrograde motion. *Geology, 27*(10), 955-958. https://doi.org/10.1130/0091-7613(1999)027<0955:EBITTB>2.3.CO;2

Chen, X. L., Ran, H. L., & Yang, W. T. (2012). Evaluation of factors controlling large earthquake-induced landslides by the Wenchuan earthquake. *Natural Hazards and Earth System Sciences, 12*(12), 3645-3657. https://doi.org/10.5194/nhess-12-3645-2012

Chiodini, G., Cardellini, C., Amato, A., Boschi, E., Caliro, S., Frondini, F., & Ventura, G. (2004). Carbon dioxide Earth degassing and seismogenesis in central and southern Italy. *Geophysical Research Letters*, 31(7). https://doi.org/10.1029/2004GL019480.

Chiodini, G., Cardellini, C., Di Luccio, F., Selva, J., Frondini, F., Caliro, S., et al. (2020). Correlation between tectonic CO2 Earth degassing and seismicity is revealed by a 10-year record in the Apennines, Italy. *Science Advances*, 6(35), eabc2938. https://doi.org/10.1126/sciadv.abc2938

Cinti, F. R., D'Addezio, G., Pantosti, D., & Hamilton, J. (1992). Ricostruzione topografica di dettaglio della scarpata di faglia del Piano di Pezza, Abruzzo. *Studi Geologici Camerti, 12*, 115-122.

Cinti, F. R., Pantosti, D., Martini, P. M. D., Pucci, S., Civico, R., Pierdominici, S., et al. (2011). Evidence for surface faulting events along the Paganica fault prior to the 6 April 2009 L'Aquila earthquake (central Italy). *Journal of Geophysical Research, 116,* B07308, doi:10.1029/2010JB007988.Cowie, P. A., Phillips, R. J., Roberts, G. P., McCaffrey, K., Zijerveld, L. J. J., Gregory, L. C., et al. (2017). Orogen-scale uplift in the central Italian Apennines drives episodic behaviour of earthquake faults. *Scientific Reports, 7*, 44858. Article. https://doi.org/10.1038/srep44858

Cowie, P. A., & Scholz, C. H. (1992). Displacement-length scaling relationship for faults: data synthesis and discussion. *Journal of Structural Geology, 14*(10), 1149-1156. https://doi.org/10.1016/0191-8141(92)90066-6

Cyr, A. J., & Granger, D. E. (2008). Dynamic equilibrium among erosion, river incision, and coastal uplift in the northern and central Apennines, Italy. *Geology*(2), 103-106. https://doi.org/10.1130/G24003A.1

D'Addezio, G., Masana, E., & Pantosti, D. (2001). The Holocene paleoseismicity of the Aremogna-Cinque Miglia Fault (Central Italy). *Journal of Seismology, 5*(2), 181-205. journal article. https://doi.org/10.1023/A:1011403408568

Darvill, C. M. (2013). Cosmogenic nuclide analysis. In S. J. Cook, L. E. Clarke, & J. M. Nield (Eds.), *Geomorphological Techniques (Online Edition)* (pp. 1-25). London, UK: British Society for Geomorphology.

Devoti, R., D'Agostino, N., Serpelloni, E., Pietrantonio, G., Riguzzi, F., Avallone, A., et al. (2017). A Combined Velocity Field of the Mediterranean Region. *Annals of Geophysics, 60*(2). GPS; crustal motion; mediterranean. https://doi.org/10.4401/ag-7059

Di Naccio, D., Kastelic, V., Carafa, M. M. C., Esposito, C., Milillo, P., & Di Lorenzo, C. (2019). Gravity versus Tectonics: the case of 2016 Amatrice and Norcia (central Italy) earthquakes surface coseismic fractures. *Journal of Geophysical Research: Earth Surface,* 124, 994– 1017. https://doi.org/10.1029/2018JF004762

Doglioni, C., Barba, S., Carminati, E., & Riguzzi, F. (2011). Role of the brittle-ductile transition on fault activation. *Physics of the Earth and Planetary Interiors*, 184, 160-171.

Falcucci, E., Gori, S., Moro, M., Fubelli, G., Saroli, M., Chiarabba, C., & Galadini, F. (2015). Deep reaching versus vertically restricted Quaternary normal faults: Implications on seismic potential assessment in tectonically active regions: Lessons from the middle Aterno valley fault system, central Italy. *Tectonophysics, 651-652*, 186-198. https://doi.org/10.1016/j.tecto.2015.03.021

Faure Walker, J. P., Roberts, G. P., Cowie, P. A., Papanikolaou, I. D., Sammonds, P. R., Michetti, A. M., & Phillips, R. J. (2009). Horizontal strain-rates and throw-rates across breached relay zones, central Italy: Implications for the preservation of throw deficits at points of normal fault linkage. *Journal of Structural Geology, 31*(10), 1145-1160. https://doi.org/10.1016/j.jsg.2009.06.011

Faure Walker, J. P., Roberts, G. P., Sammonds, P. R., & Cowie, P. (2010). Comparison of earthquake strains over 102 and 104 year timescales: Insights into variability in the seismic cycle in the central Apennines, Italy. *Journal of Geophysical Research: Solid Earth, 115*(B10). https://doi.org/10.1029/2009JB006462

Faure Walker, J. P., Visini, F., Roberts, G., Galasso, C., McCaffrey, K., & Mildon, Z. (2019). Variable Fault Geometry Suggests Detailed Fault-Slip-Rate Profiles and Geometries Are Needed for Fault-Based Probabilistic Seismic Hazard Assessment (PSHA). *Bulletin of the Seismological Society of America, 109*(1), 110-123. https://doi.org/10.1785/0120180137

Field, E. H., Arrowsmith, R. J., Biasi, G. P., Bird, P., Dawson, T. E., Felzer, K. R., et al. (2014). Uniform California Earthquake Rupture Forecast, Version 3 (UCERF3)—The Time-Independent Model. *Bulletin of the Seismological Society of America, 104*(3), 1122-1180. https://doi.org/10.1785/0120130164

Galadini, F. (1999). Pleistocene changes in the central Apennine fault kinematics: A key to decipher active tectonics in central Italy. *Tectonics, 18*(5), 877-894. https://doi.org/10.1029/1999TC900020

Galadini, F. (2006). Quaternary tectonics and large-scale gravitational deformations with evidence of rock-slide displacements in the Central Apennines (central Italy). *Geomorphology, 82*(3-4), 201-228. https://doi.org/10.1016/j.geomorph.2006.05.003

Galadini, F., & Galli, P. (1999). The Holocene paleoearthquakes on the 1915 Avezzano earthquake faults (central Italy): implications for active tectonics in the central Apennines. *Tectonophysics, 308*, 143-170.

Galadini, F., & Galli, P. (2000). Active Tectonics in the Central Apennines (Italy) – Input Data for Seismic Hazard Assessment. *Natural Hazards, 22*(3), 225-268. journal article. https://doi.org/10.1023/A:1008149531980

Galadini, F., Giraudi, C., & Messina, P. (1998). Nuovi dati sulla tettonica tardopleistocenica dell'alta valle del Sangro (Appennino centrale): implicazioni sismotettoniche. *Il Quaternario, 11*, 347-356.

Galli, P. (2020). Recurrence times of central-southern Apennine faults (Italy): hints from paleoseismology. *Terra Nova*(n/a). https://doi.org/10.1111/ter.12470

Galli, P., Galadini, F., & Pantosti, D. (2008). Twenty years of paleoseismology in Italy. *Earth-Science Reviews, 88*, 89-117.

Galli, P., Giaccio, B., & Messina, P. (2010). The 2009 central Italy earthquake seen through 0.5 Myr-long tectonic history of the L'Aquila faults system. *Quaternary Science Reviews, 29*, 3768-3789.

Galli, P., Giaccio, B., Peronace, E., & Messina, P. (2015). Holocene Paleoearthquakes and Early–Late Pleistocene Slip Rate on the Sulmona Fault (Central Apeninnes, Italy)Holocene Paleoearthquakes and Early–Late Pleistocene Slip Rate on the Sulmona Fault (Central Apeninnes, Italy). *Bulletin of the Seismological Society of America, 105*(1), 1-13. https://doi.org/10.1785/0120140029

Giraudi, C. (1988). Evoluzione geologica della piana del Fucino (Abruzzo) negli ultimi 30.000 anni. *Il Quaternario, 2*, 131-159.

Giraudi, C. (1989). Datazione di un evento sismico preistorico con metodi geologici e radiometrici: Piani di Aremogna e delle Cinque Miglia. In E. Guidoboni (Ed.), *I terremoti prima del Mille in Italia e nell'area mediterranea* (pp. 53-64). Bologna: ING and SGA.

Giraudi, C. (1995). Considerations on the significance of some post-glacial fault scarps in the Abruzzo Apennines (central Italy). *Quaternary International, 25*, 33-45.

Giraudi, C., & Frezzotti, M. (1995). Palaeoseismicity in the Gran Sasso Massif (Abruzzo, Central Italy). *Quaternary International, 25*, 81-93. https://doi.org/10.1016/1040-6182(94)P3716-L

Giraudi, C., & Frezzotti, M. (1997). Late Pleistocene Glacial Events in the Central Apennines, Italy. *Quaternary Research, 48*(3), 280-290. https://doi.org/10.1006/qres.1997.1928

Goodall, H. J., Gregory, L. C., Wedmore, L. N. J., McCaffrey, K. J. W., Amey, R. M. J., Roberts, G. P., et al. (2021). Determining Histories of Slip on Normal Faults With Bedrock Scarps Using Cosmogenic Nuclide Exposure Data. *Tectonics, 40*(3), e2020TC006457. https://doi.org/10.1029/2020TC006457.

Gori, S., Dramis, F., Galadini, F., & Messina, P. (2007). The use of geomorphological markers in the footwall of active faults for kinematic evaluations; examples from the Central Apennines. *Italian Journal of Geosciences, 126*(2), 365-374.

Gori, S., Giaccio, B., Galadini, F., Falcucci, E., Messina, P., Sposato, A., & Dramis, F. (2011). Active normal faulting along the Mt. Morrone south-western slopes (central Apennines, Italy). *International Journal of Earth Sciences, 100*(1), 157-171. journal article. https://doi.org/10.1007/s00531-009-0505-6

Granger, D. E., Lifton, N. A., & Willenbring, J. K. (2013). A cosmic trip: 25 years of cosmogenic nuclides in geology. *GSA Bulletin, 125*(9-10), 1379-1402. https://doi.org/10.1130/B30774.1

Kastelic, V., Burrato, P., Carafa, M. M. C., & Basili, R. (2017). Repeated surveys reveal nontectonic exposure of supposedly active normal faults in the central Apennines, Italy. *Journal of Geophysical Research-Earth Surface, 122*(1), 114-129. https://doi.org/10.1002/2016JF003953

Kastelic, V., Carafa, M. M. C., & Visini, F. (2016). Neotectonic deformation models for probabilistic seismic hazard: a study in the External Dinarides. *Geophysical Journal International, 205*(3), 1694-1709. https://doi.org/10.1093/gji/ggw106

Manighetti, I., King, G. C. P., Gaudemer, Y., Scholz, C. H., & Doubre, C. (2001). Slip accumulation and lateral propagation of active normal faults in Afar. *Journal of Geophysical Research: Solid Earth, 106*(B7), 13667-13696. https://dx.doi.org/10.1029/2000jb900471

McCalpin, J. (2009). *Paleoseismology (2nd ed.)*. San Diego, USA: Academic Press, Elsevier Publishing.

McPhillips, D., & Scharer, K. M. (2018). Quantifying Uncertainty in Cumulative Surface Slip Along the Cucamonga Fault, a Crustal Thrust Fault in Southern California. *Journal of Geophysical Research: Solid Earth, 123*(10), 9063-9083. https://doi.org/10.1029/2018JB016301.

Miccadei, E., Piacentini, T., & Barberi, R. (2002). Uplift and local tectonic subsidence in the evolution of intramontane basins: the example of the Sulmona basin (central Apennines). *Studi Geologici Camerti, vol. spec.*, 119-133.

Michetti, A. M., Brunamonte, F., Serva, L., & Vittori, E. (1996). Trench investigations of the 1915 Fucino earthquake fault scarps (Abruzzo, central Italy): Geological evidence of large historical events. *Journal of Geophysical Research: Solid Earth, 101*(B3), 5921-5936. https://doi.org/10.1029/95JB02852

Morell, K. D., Styron, R., Stirling, M., Griffin, J., Archuleta, R., & Onur, T. (2020). Seismic Hazard Analyses From Geologic and Geomorphic Data: Current and Future Challenges. *Tectonics, 39*(10), e2018TC005365. https://doi.org/10.1029/2018TC005365

Morewood, N. C., & Roberts, G. P. (2000). The geometry, kinematics and rates of deformation within an en echelon normal fault segment boundary, central Italy. *Journal of Structural Geology, 22*(8), 1027-1047. https://doi.org/10.1016/S0191-8141(00)00030-4

Moro, M., Gori, S., Falcucci, E., Saroli, M., Galadini, F., & Salvi, S. (2013). Historical earthquakes and variable kinematic behaviour of the 2009 L'Aquila seismic event (central Italy) causative fault, revealed by paleoseismological investigations. *Tectonophysics, 583*, 131-144. https://doi.org/10.1016/j.tecto.2012.10.036

Murru, M., Falcone, G., Taroni, M., & Console, R. (2020). Application of an ensemble earthquake rate model in Italy, considering seismic catalogs and fault moment release. *Annals of Geophysics, 63*(6). https://doi.org/10.4401/ag-8441

Pantosti, D., D'Addezio, G., & Cinti, F. R. (1996). Paleoseismicity of the Ovindoli-Pezza fault, central Apennines, Italy: A history including a large, previously unrecorded earthquake in the Middle Ages (860-1300 A.D.). *Journal of Geophysical Research: Solid Earth, 101*(B3), 5937-5959. http://dx.doi.org/10.1029/95JB03213

Papanikolaou, I. D., Roberts, G. P., & Michetti, A. M. (2005). Fault scarps and deformation rates in Lazio–Abruzzo, Central Italy: Comparison between geological fault slip-rate and GPS data. *Tectonophysics, 408*(1-4), 147-176. https://doi.org/10.1016/j.tecto.2005.05.043

Patruno, S., & Scisciani, V. (2021). Testing normal fault growth models by seismic stratigraphic architecture: The case of the Pliocene-Quaternary Fucino Basin (Central Apennines, Italy). *Basin Research, 33*(3), 2118-2156. https://doi.org/10.1111/bre.12551.

Peacock, D. C. P., & Sanderson, D. J. (1991). Displacements, segment linkage and relay ramps in normal fault zones. *Journal of Structural Geology, 13*(6), 721-733. https://doi.org/10.1016/0191-8141(91)90033-F

Piacentini, T., & Miccadei, E. (2014). The role of drainage systems and intermontane basins in the Quaternary landscape of the Central Apennines chain (Italy). *Rendiconti Lincei, 25*(2), 139-150. https://doi.org/10.1007/s12210-014-0312-2

Piccardi, L., Gaudemer, Y., Tapponnier, P., & Boccaletti, M. (1999). Active oblique extension in the central Apennines (Italy): evidence from the Fucino region. *Geophysical Journal International, 139*, 499-530.

Pizzi, A., Calamita, F., Coltorti, M., & Pieruccini, P. (2002). Quaternary normal faults , intramontane basins and seismicity in the Umbria-Marche-Abruzzi Apennine Ridge (Italy): contribution of neotectonic analysis to seismic hazard assessment. *Bollettino Societa'Geologica Italiana Spec. Pub., 1*, 923-929.

Pizzi, A., Falcucci, E., Gori, S., Galadini, F., Messina, P., Di Vincenzo, M., et al. (2010). Active faulting in the Maiella Massif (central Apennines, Italy). *GeoActa, Special Publication, 3*, 57-73.

Pizzi, A., & Pugliese, G. (2004). InSAR-DEM analyses integrated with geologic field methods for the study of long-term seismogenic fault behavior: Applications in the axial zone of the central Apennines (Italy). *Journal of Seismology, 8*(3), 313-329. https://doi.org/10.1023/B:JOSE.0000038454.18706.25

Pucci, S., Civico, R., Villani, F., Ricci, T., Delcher, E., Finizola, A., et al. (2016). Deep electrical resistivity tomography along the tectonically active Middle Aterno Valley (2009 L'Aquila earthquake area, central Italy). *Geophysical Journal International, 207*(2), 967-982. https://doi.org/10.1093/gji/ggw308

Pucci, S., Villani, F., Civico, R., Di Naccio, D., Porreca, M., Benedetti, L., et al. (2019). Complexity of the 2009 L'Aquila earthquake causative fault system (Abruzzi Apennines, Italy) and effects on the Middle Aterno Quaternary basin arrangement. *Quaternary Science Reviews, 213*, 30-66. https://doi.org/10.1016/j.quascirev.2019.04.014

Roback, K., Clark, M. K., West, A. J., Zekkos, D., Li, G., Gallen, S. F., et al. (2018). The size, distribution, and mobility of landslides caused by the 2015 Mw7.8 Gorkha earthquake, Nepal. *Geomorphology, 301*, 121-138. https://doi.org/10.1016/j.geomorph.2017.01.030

Roberts, G. P., & Michetti, A. M. (2004). Spatial and temporal variations in growth rates along active normal fault systems: an example from The Lazio–Abruzzo Apennines, central Italy. *Journal of Structural Geology, 26*(2), 339-376. https://doi.org/10.1016/S0191-8141(03)00103-2

Roberts, G. P., Raithatha, B., Sileo, G., Pizzi, A., Pucci, S., Walker, J. F., et al. (2010). Shallow subsurface structure of the 2009 April 6 Mw 6.3 L'Aquila earthquake surface rupture at Paganica, investigated with ground-penetrating radar. *Geophysical Journal International, 183*(2), 774-790. https://doi.org/10.1111/j.1365-246X.2010.04713.x

Salvi, S., Cinti, F. R., Colini, L., D'Addezio, G., Doumaz, F., & Pettinelli, E. (2003). Investigation of the active Celano–L'Aquila fault system, Abruzzi (central Apennines, Italy) with combined ground-penetrating radar and palaeoseismic trenching. *Geophysical Journal International, 155*(3), 805-818. https://doi.org/10.1111/j.1365-246X.2003.02078.x

Saroli, M., Moro, M., Borghesi, H., Dell'Acqua, D., Galadini, F., & Galli, P. (2008). Nuovi dati paleoseismologici del settore orientale del bacino del Fucino (Italia centrale). *Il Quaternario, 21*, 383-394.

Schirripa Spagnolo, G., Mercuri, M., Billi, A., Carminati, E., & Galli, P. (2021). The Segmented Campo Felice Normal Faults: Seismic Potential Appraisal by Application of Empirical Relationships Between Rupture Length and Earthquake Magnitude in the Central Apennines, Italy. *Tectonics*, 40(7), e2020TC006465. https://doi.org/10.1029/2020TC006465.

Schlagenhauf, A. (2009). *Identication des forts séismes passés sur les failles normales actives de la région Lazio-Abruzzo (Italie Centrale) par `datations cosmogéniques' (36Cl) de leurs escarpements.* (Docteur de l'Université Joseph Fourier, spécialité « Terre – Univers – Environnement » PhD), Université Joseph Fourier Grenoble-France. Retrieved from https://tel.archives-ouvertes.fr/tel-00461004

Schlagenhauf, A., Gaudemer, Y., Benedetti, L., Manighetti, I., Palumbo, L., Schimmelpfennig, I., et al. (2010). Using in situ Chlorine-36 cosmonuclide to recover past earthquake histories on limestone normal fault scarps: a reappraisal of methodology and interpretations. *Geophysical Journal International, 182*(1), 36-72. https://doi.org/10.1111/j.1365-246X.2010.04622.xSchlagenhauf, A., Manighetti, I., Benedetti, L., Gaudemer, Y., Finkel, R., Malavieille, J., & Pou, K. (2011). Earthquake supercycles in Central Italy, inferred from 36Cl exposure dating. *Earth and Planetary Science Letters, 307*(3), 487-500. https://doi.org/10.1016/j.epsl.2011.05.022

Scholz, C. H., & Lawler, T. M. (2004). Slip tapers at the tips of faults and earthquake ruptures. *Geophysical Research Letters, 31*(21). https://doi.org/10.1029/2004GL021030.

Serva, L., Blumetti, A. M., & Michetti, A. M. (1986). Gli effetti sul terreno del terremoto del Fucino (13 Gennaio 1915); tentativo di interpretazione della evoluzione tettonica recente di alcune strutture. *Mem. Soc. Geol. It, 35*, 893-907.

Smeraglia, L., Bernasconi, S. M., Berra, F., Billi, A., Boschi, C., Caracausi, A., et al. (2018). Crustal-scale fluid circulation and co-seismic shallow comb-veining along the longest normal fault of the

central Apennines, Italy. Earth and Planetary Science Letters, 498, 152-168. https://doi.org/10.1016/j.epsl.2018.06.013

Smeraglia, L., Bettucci, A., Billi, A., Carminati, E., Cavallo, A., Di Toro, G., et al. (2017). Microstructural evidence for seismic and aseismic slips along clay-bearing, carbonate faults. Journal of Geophysical Research: Solid Earth, 122(5), 3895-3915. https://doi.org/10.1002/2017JB014042.

Stemberk, J., Moro, G. D., Stemberk, J., Blahůt, J., Coubal, M., Košťák, B., et al. (2019). Strain monitoring of active faults in the central Apennines (Italy) during the period 2002–2017. *Tectonophysics, 750*, 22-35. https://doi.org/10.1016/j.tecto.2018.10.033

Styron, R. (2019). The impact of earthquake cycle variability on neotectonic and paleoseismic slip rate estimates. *Solid Earth, 10*(1), 15-25. https://doi.org/10.5194/se-10-15-2019

Tesson, J., Pace, B., Benedetti, L., Visini, F., Delli Rocioli, M., Arnold, M., et al. (2016). Seismic slip history of the Pizzalto fault (central Apennines, Italy) using in situ-produced 36Cl cosmic ray exposure dating and rare earth element concentrations. *Journal of Geophysical Research: Solid Earth, 121*(3), 1983-2003. https://doi.org/10.1002/2015JB012565.

Tucker, G. E., McCoy, S. W., Whittaker, A. C., Roberts, G. P., Lancaster, S. T., & Phillips, R. (2011). Geomorphic significance of postglacial bedrock scarps on normal-fault footwalls. *Journal of Geophysical Research: Earth Surface, 116*(F1). https://doi.org/10.1029/2010JF001861

Villani, F., Tulliani, V., Sapia, V., Fierro, E., Civico, R., & Pantosti, D. (2015). Shallow subsurface imaging of the Piano di Pezza active normal fault (central Italy) by high-resolution refraction and electrical resistivity tomography coupled with time-domain electromagnetic data. *Geophysical Journal International, 203*(3), 1482-1494. https://doi.org/10.1093/gji/ggv399

Visini, F., Pace, B., Meletti, C., Marzocchi, W., Akinci, A., Azzaro, R., et al. (2021). Earthquake Rupture Forecasts for the MPS19 Seismic Hazard Model of Italy. *Ann. Geophys, 64*(2).

Wilkinson, M., Roberts, G. P., McCaffrey, K., Cowie, P. A., Walker, J. P. F., Papanikolaou, I., et al. (2015). Slip distributions on active normal faults measured from LiDAR and field mapping of geomorphic offsets: an example from L'Aquila, Italy, and implications for modelling seismic moment release. *Geomorphology, 237*, 130-141. https://doi.org/10.1016/j.geomorph.2014.04.026

Captions

Figure 1. Map of the active faults and measurement points across the central Apennines. The measurement points are distinguished by used technique: LGMA = Last Glacial Maximum; CHEA = geochemical analysis in scarps; LONG = long-term geologic offsets; TRCH = paleoseismic trenching. Refer to the Table S1 for fault code, offset, and age of each measurement.

Figure 2. Plots of samples of different types of probability density functions (PDFs) used for both throw (ΔF) and age (Δt) distributions.

Figure 3. Frequency distribution of paleoearthquake throws in the central Apennines. The black lines show the cumulative distributions; grey circles indicate 5^{th}, 50^{th} and 95^{th} percentiles of each distribution. The red line is the exponential function fitting the cumulative distribution of paleoearthquake throws.

Figure 4. Frequency distribution of sampled age for the complete dataset (top) and for different techniques (bottom). The black lines show the cumulative distributions; grey circles indicate 5^{th}, 50^{th} and 95^{th} percentiles of each distribution. Throw-rate measurement techniques: numerical-modeling methods applied to trace elements and cosmogenic radionuclides (CHEA), geomorphic markers exposed

since the Last Glacial Maximum (LGMA), long-term (>20 kyr) estimates (LONG), and paleoseismic trenching (TRCH).

Figure 5. Frequency distribution of throw rates for the complete dataset (top) and each method subdataset (bottom). The black lines show the cumulative distributions; grey circles indicate 5th, 50th and 95th percentiles of each distribution. Throw-rate measurement techniques: numerical-modeling methods applied to trace elements and cosmogenic radionuclides (CHEA), geomorphic markers exposed since the Last Glacial Maximum (LGMA), long-term (>20 kyr) estimates (LONG), and palesoseismic trenching (TRCH). The red line is the lognormal function fitting the cumulative distribution of throw rates.

Figure 6. 95% Confidence Level (C.L.) for both ΔF and Δt. Top: measured 95% C.L. for ΔF and tested total uncertainties $\sigma'_{\Delta F}$ (see Figure 10). Bottom: 95% C.L. for Δt and tested total uncertainties $\sigma'_{\Delta t}$.

Figure 7. Along-strike variability for different faults (see Figure 1 and Table S1 for location). The suggested throw-rate profile used in our calculation for the fault throw rate is also shown.

Figure 8. Cumulative distribution curves of disagreement δ. Bottom left: the cumulative distributions for all possible data pairs (on the same fault) are shown. Top right: distribution curves of disagreement δ disaggregated by methods. The red circles describe the fraction of highly-disagreeing data pairs ($\delta \geq 0.95$), defined in the text with the parameter β.

Figure 9. The variability of β (fraction of $\delta \geq 0.95$ data pairs) in space and time. The average value of $\beta = 0.13$ (see Figure 8) is shown with a dotted blank line, whereas blue points report the interval-average fractions.

Figure 10. Forward modeling of throw rates using different total uncertainties $\sigma'_{\Delta F}$. The optimal model B ($\sigma'_{\Delta F} = \Delta t \cdot 0.10$ mm/yr) minimizes the differences between real-data (black) and synthetic-data (grey) disagreement curves at fixed $\sigma'_{\Delta F}$. This minimization implies that collected measurements are tectonic but affected by a total throw uncertainty $\sigma'_{\Delta F}$ greater than the observational one $\sigma_{\Delta F}$. Instead, the difference between the black and red lines indicates the effect of using $\sigma'_{\Delta F}$ (total uncertainty) to $\sigma_{\Delta F}$ (observation error) in determining the probability density function of the long-term throw rates (p_L).

Figure 11. Top: Resulting uniform throw rates (Top) and relative coefficient of variation COV (Bottom). For the fault name refer to Table 1.

Table 1. Throw-rate median, 95% Confidence Interval and Coefficient of Variation (COV) for the central Apennines. See Figure 11 for linking fault ID to its location.

Figure 1.

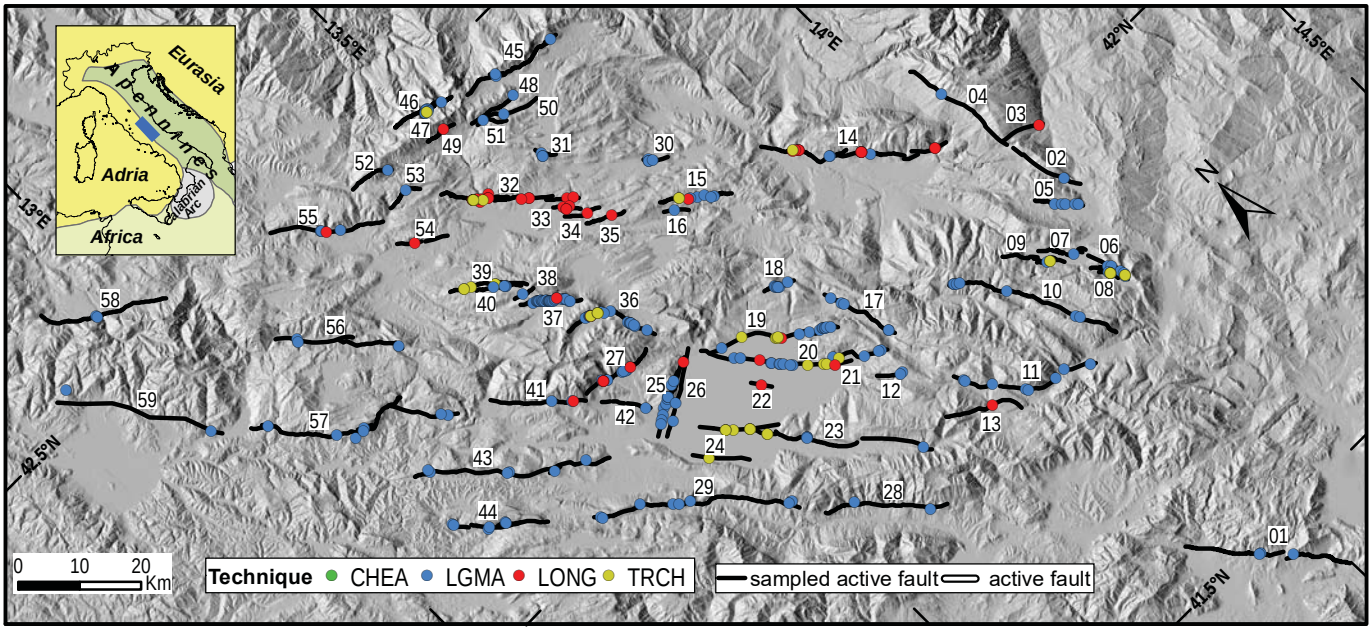
Eurasia
Apennines
Adria
Calabrian Arc
Africa
13.5°E
14°E
14.5°E
42°N
41.5°N
42.5°N
13°E
N
01
02
03
04
05
06
07
08
09
10
11
12
13
14
15
16
17
18
19
20
21
22
23
24
25
26
27
28
29
30
31
32
33
34
35
36
37
38
39
40
41
42
43
44
45
46
47
48
49
50
51
52
53
54
55
56
57
58
59
0 10 20 Km
Technique CHEA LGMA LONG TRCH
sampled active fault
active fault

Figure 2.

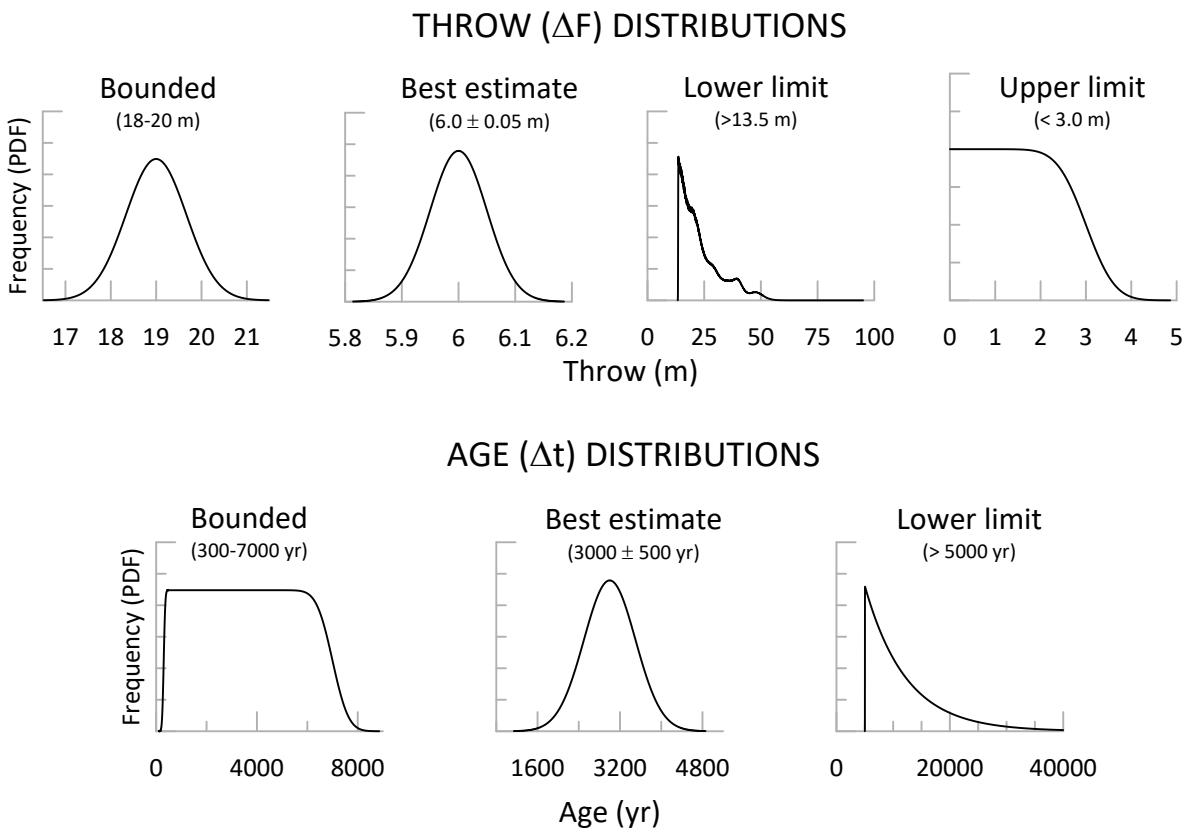
THROW (ΔF) DISTRIBUTIONS
Bounded
(18-20 m)
Best estimate
(6.0 ± 0.05 m)
Lower limit
(>13.5 m)
Upper limit
(< 3.0 m)
Frequency (PDF)
17 18 19 20 21
5.8 5.9 6 6.1 6.2
0 25 50 75 100
0 1 2 3 4 5
Throw (m)
AGE (Δt) DISTRIBUTIONS
Bounded
(300-7000 yr)
Best estimate
(3000 ± 500 yr)
Lower limit
(> 5000 yr)
Frequency (PDF)
0 4000 8000
1600 3200 4800
0 20000 40000
Age (yr)

Figure 3.

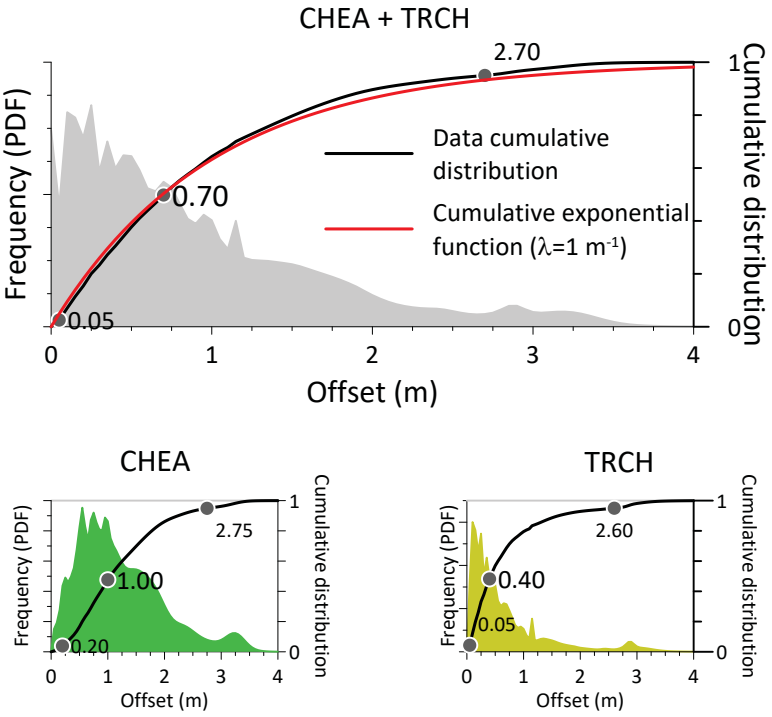
CHEA + TRCH
Frequency (PDF)
Cumulative distribution
Offset (m)
2.70
0.70
0.05
Data cumulative distribution
Cumulative exponential function (λ=1 m-1)
0
1
2
3
4
1
0
CHEA
2.75
1.00
0.20
TRCH
2.60
0.40
0.05

Figure 4.

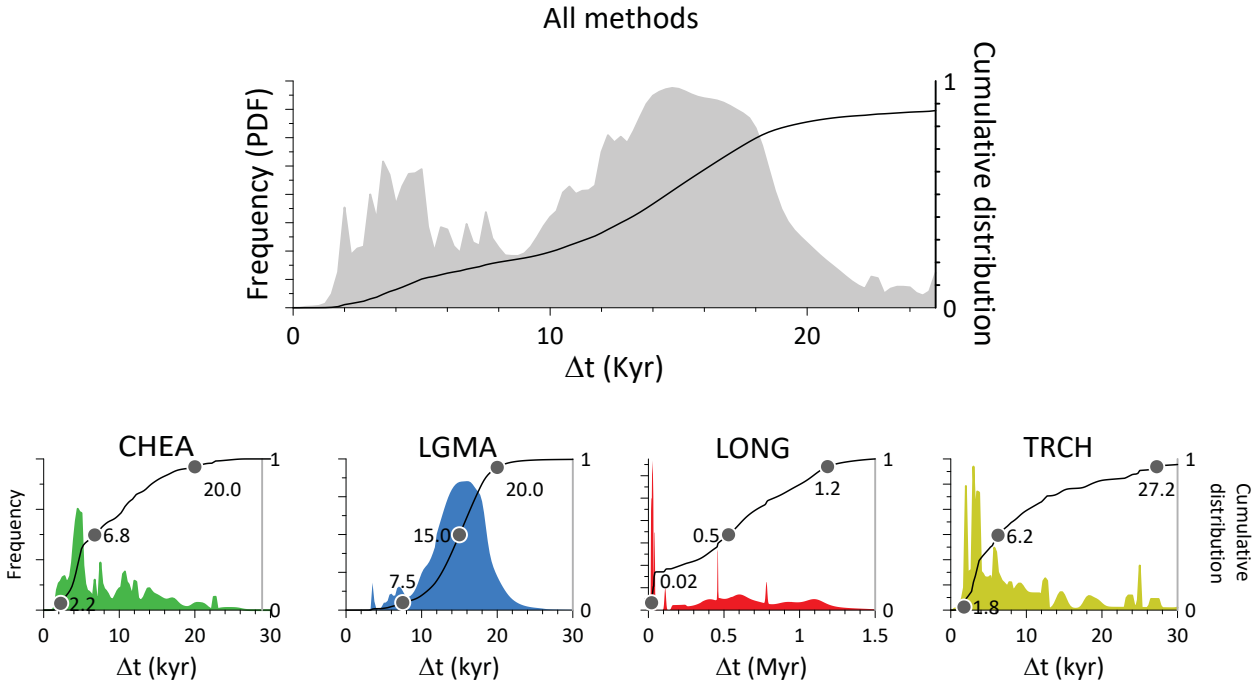
All methods
Frequency (PDF)
Cumulative distribution
0
10
20
Δt (Kyr)
1
0
CHEA
LGMA
LONG
TRCH
Frequency
Cumulative distribution
20.0
6.8
2.2
15.0
7.5
1.2
0.5
0.02
27.2
6.2
1.8
Δt (kyr)
Δt (Myr)

Figure 5.

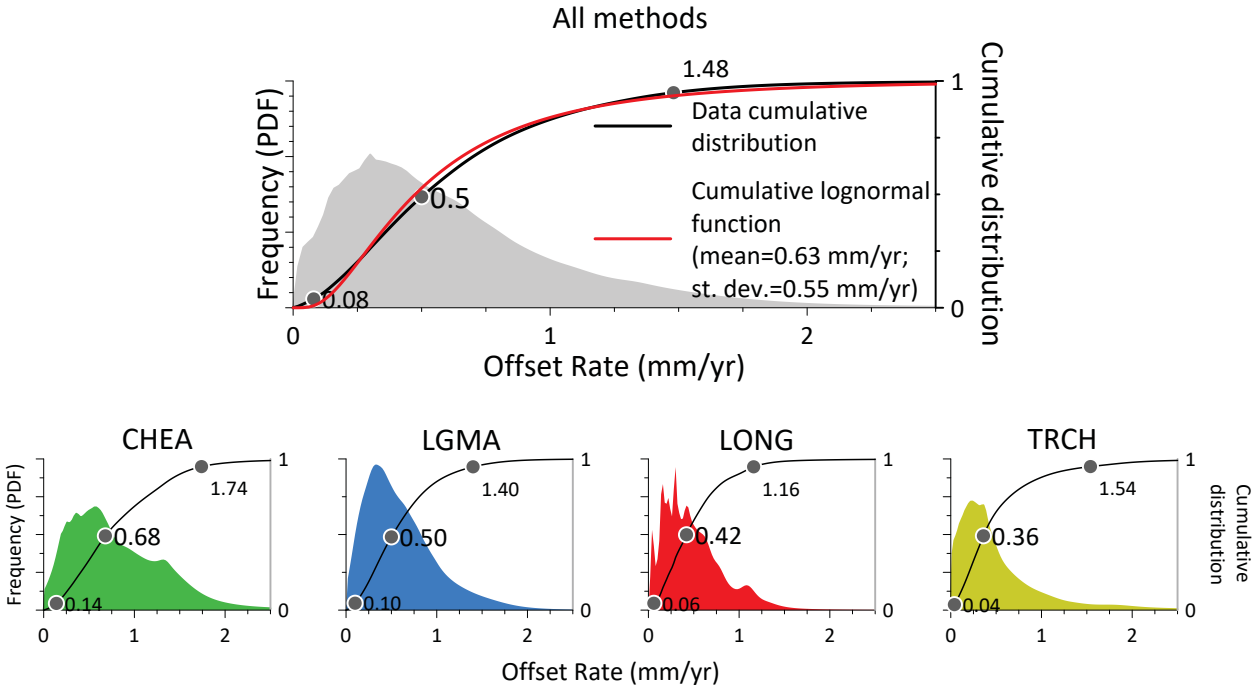
All methods
Frequency (PDF)
Cumulative distribution
1.48
0.5
0.08
Data cumulative distribution
Cumulative lognormal function
(mean=0.63 mm/yr;
st. dev.=0.55 mm/yr)
Offset Rate (mm/yr)
CHEA
1.74
0.68
0.14
LGMA
1.40
0.50
0.10
LONG
1.16
0.42
0.06
TRCH
1.54
0.36
0.04
Offset Rate (mm/yr)

Figure 6.

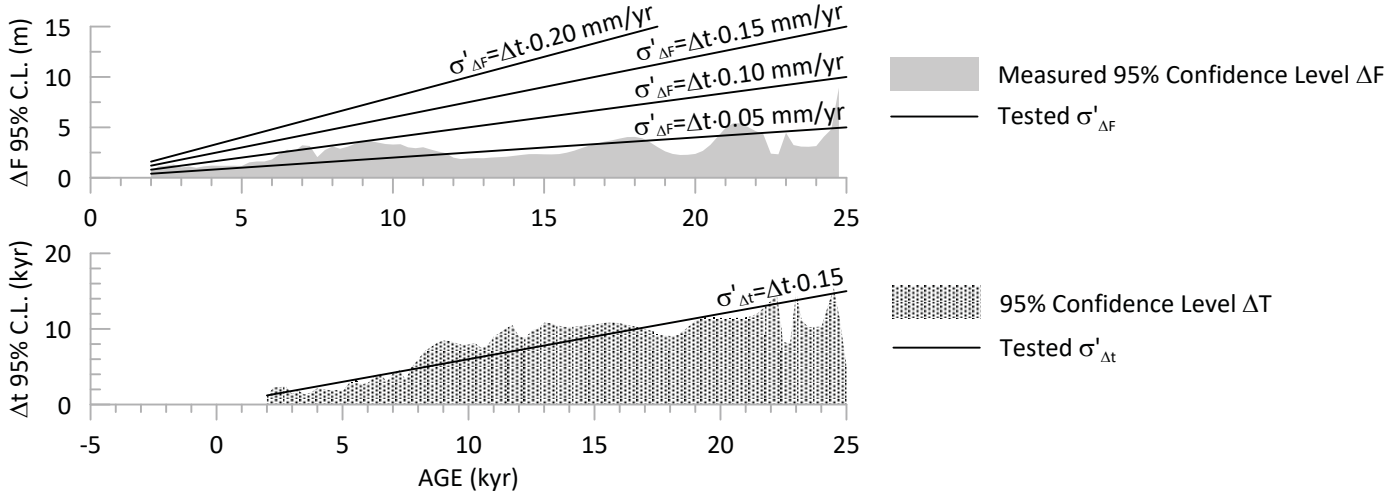
ΔF 95% C.L. (m)
15
10
5
0
σ'ΔF=Δt·0.20 mm/yr
σ'ΔF=Δt·0.15 mm/yr
σ'ΔF=Δt·0.10 mm/yr
σ'ΔF=Δt·0.05 mm/yr
0
5
10
15
20
25
Δt 95% C.L. (kyr)
20
10
0
σ'Δt=Δt·0.15
-5
0
5
10
15
20
25
AGE (kyr)
Measured 95% Confidence Level ΔF
Tested σ'ΔF
95% Confidence Level ΔT
Tested σ'Δt

Figure 7.

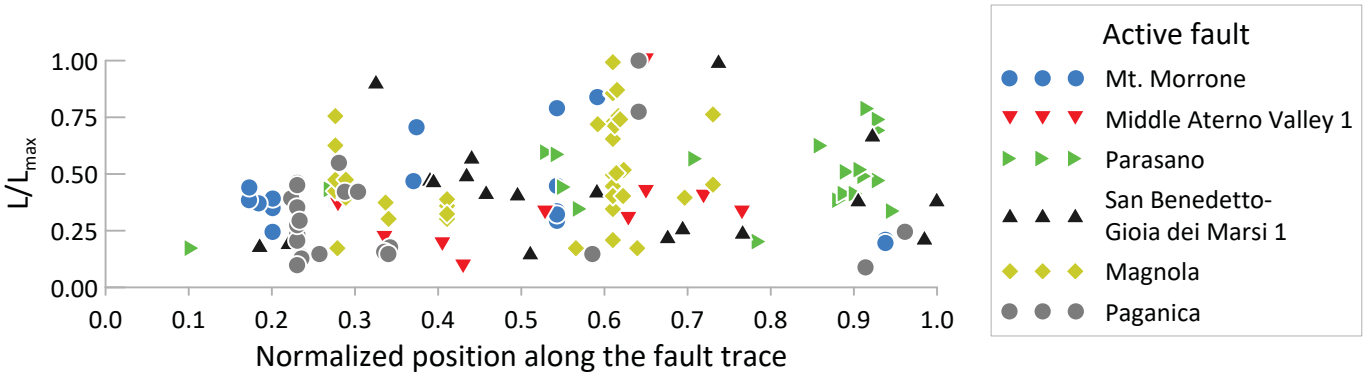
1.00
0.75
0.50
0.25
0.00
L/Lmax
0.0
0.1
0.2
0.3
0.4
0.5
0.6
0.7
0.8
0.9
1.0
Normalized position along the fault trace
Active fault
Mt. Morrone
Middle Aterno Valley 1
Parasano
San Benedetto-Gioia dei Marsi 1
Magnola
Paganica

Figure 8.

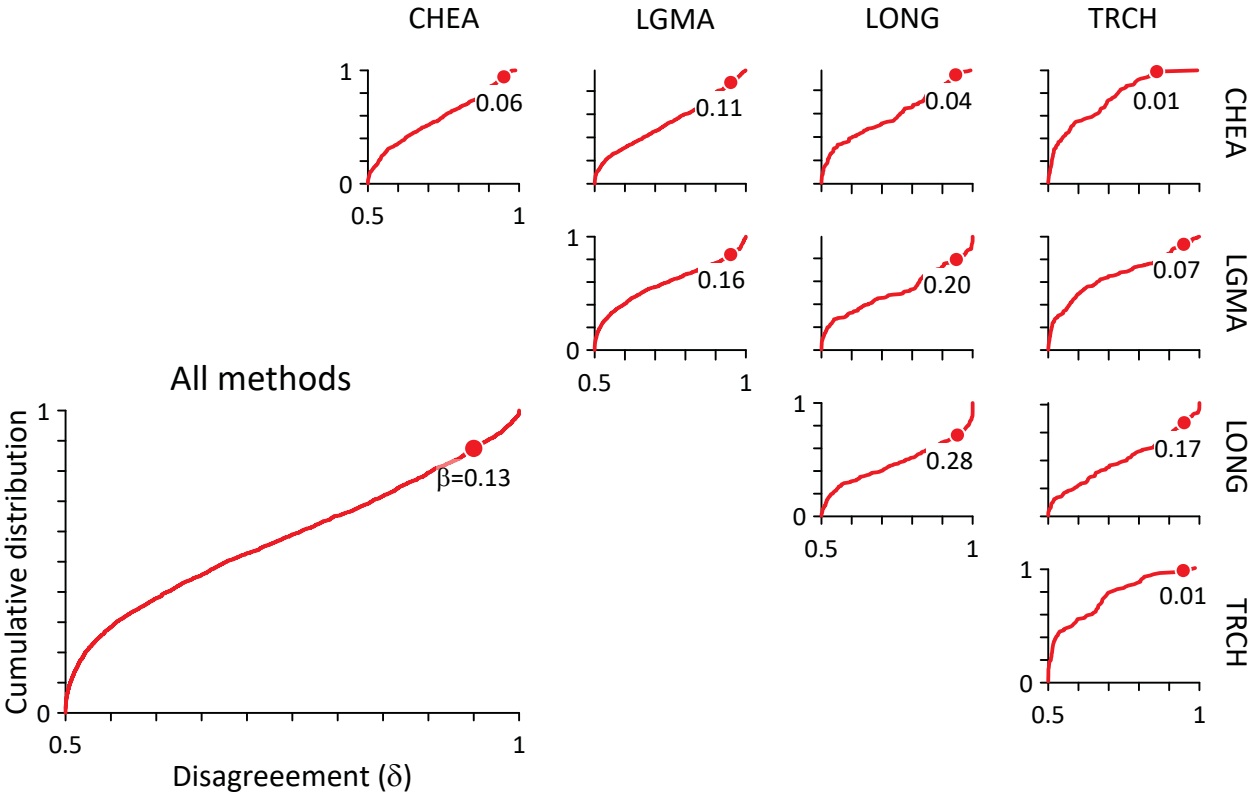
CHEA
LGMA
LONG
TRCH
All methods
Cumulative distribution
Disagreeement (δ)
β=0.13
0.06
0.11
0.04
0.01
0.16
0.20
0.07
0.28
0.17
0.01
0
0.5
1

Figure 9.

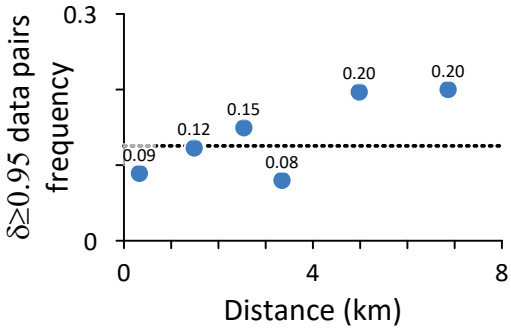
δ≥0.95 data pairs frequency
0.3
0
0
4
8
Distance (km)
0.09
0.12
0.15
0.08
0.20
0.20

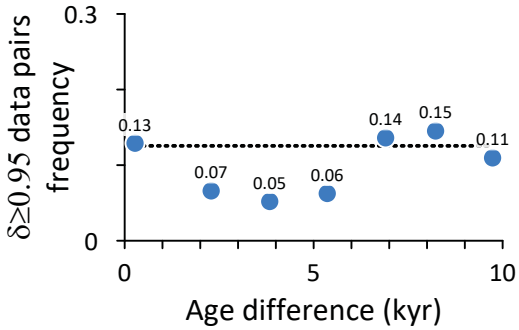
δ≥0.95 data pairs frequency
0.3
0
0
5
10
Age difference (kyr)
0.13
0.07
0.05
0.06
0.14
0.15
0.11

Figure 10.

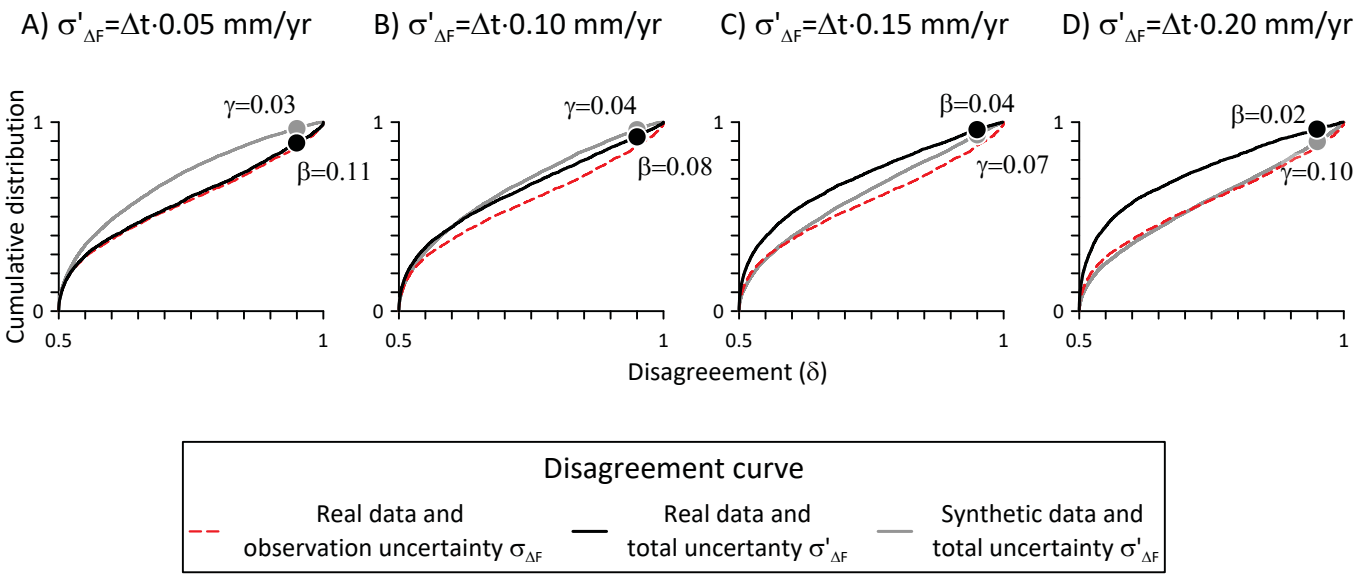
A) σ'ΔF=Δt·0.05 mm/yr
B) σ'ΔF=Δt·0.10 mm/yr
C) σ'ΔF=Δt·0.15 mm/yr
D) σ'ΔF=Δt·0.20 mm/yr
Cumulative distribution
γ=0.03
β=0.11
γ=0.04
β=0.08
β=0.04
γ=0.07
β=0.02
γ=0.10
0
0.5
1
Disagreeement (δ)
Disagreement curve
Real data and observation uncertainty σΔF
Real data and total uncertanty σ'ΔF
Synthetic data and total uncertainty σ'ΔF

Figure 11.

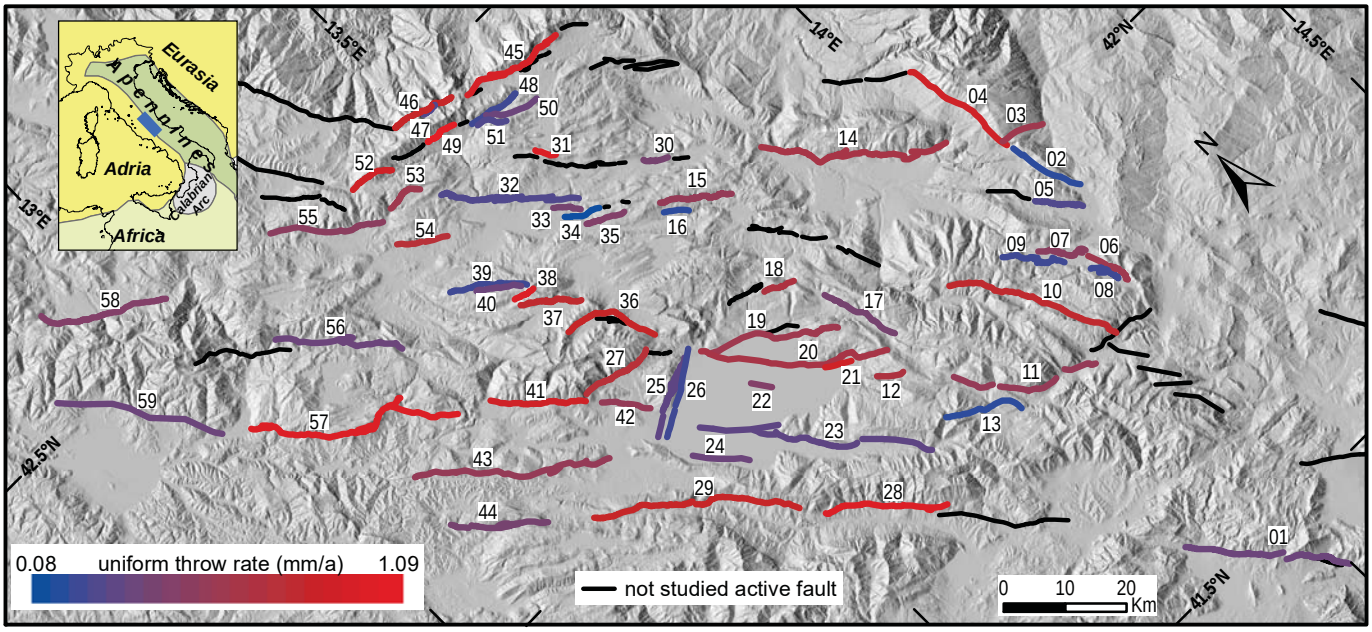
Eurasia
Apennines
Adria
Calabrian Arc
Africa
13.5°E
14°E
14.5°E
42°N
42.5°N
41.5°N
13°E
N
0.08 uniform throw rate (mm/a) 1.09
not studied active fault
0 10 20 Km

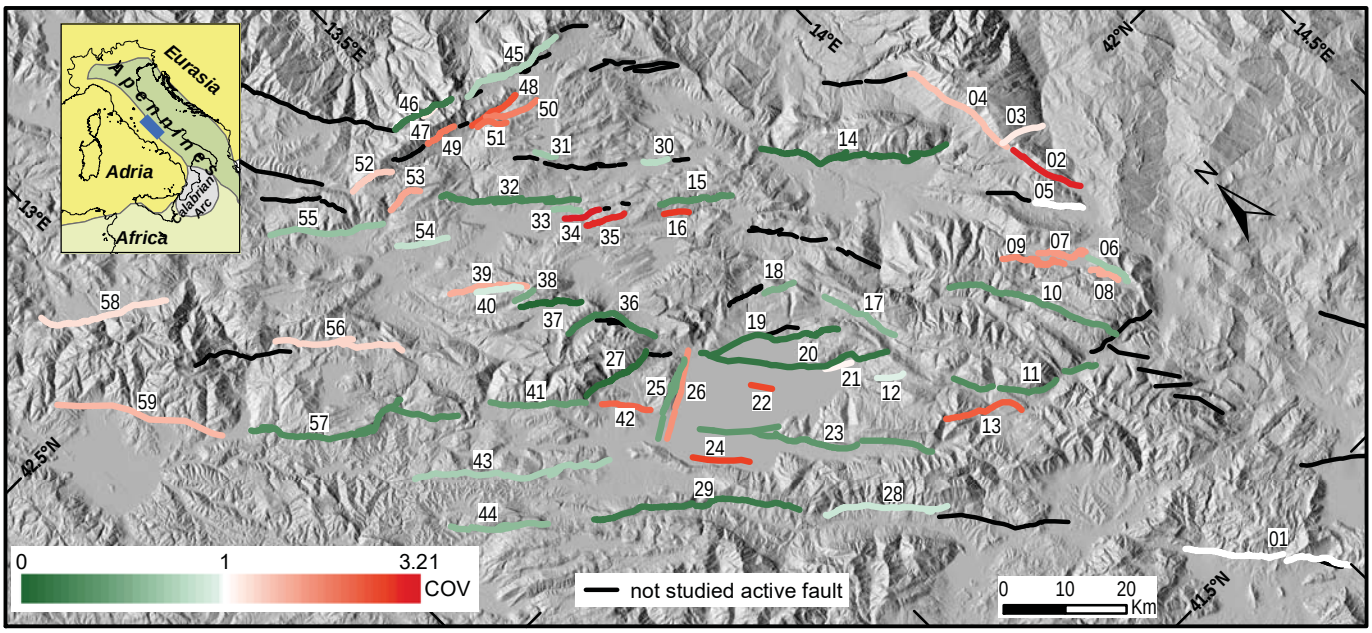
Eurasia
Apennines
Adria
Calabrian Arc
Africa
13.5°E
14°E
14.5°E
42°N
42.5°N
41.5°N
13°E
N
0 1 3.21 COV
not studied active fault
0 10 20 Km

Table 1. Throw-rate median, 95% Confidence Interval and Coefficient of Variation (COV) for the central Apennines. See Figure 11 for linking fault ID to its location.

Fault ID	Fault name	Median (mm/yr)	95% Confidence Interval (mm/yr)	COV	Measurements (#)
1	Cassino	0.32	0.17-0.50	1.00	3
2	Porrara	0.14	0.01-0.44	2.99	1
3	Maiella-Palena	0.47	0.26-0.75	1.05	1
4	Maiella-Caramanico	0.83	0.49-1.46	1.17	1
5	Pizzalto	0.24	0.13-0.37	1.00	8
6	Aremogna-Cinque Miglia 1	0.46	0.31-0.63	0.70	7
7	Aremogna-Cinque Miglia 2	0.41	0.10-0.73	1.55	1
8	Aremogna-Cinque Miglia 3	0.21	0.06-0.37	1.47	5
9	Aremogna-Cinque Miglia 4	0.21	0.05-0.41	1.69	3
10	Scanno	0.75	0.58-0.95	0.48	8
11	Sangro-Mt. Marsicano 1	0.44	0.34-0.55	0.46	9
12	Sangro-Mt. Marsicano 2	0.52	0.31-0.80	0.94	2
13	Sangro-Mt. Marsicano 3	0.16	0.02-0.40	2.44	1
14	Mt. Morrone	0.49	0.41-0.57	0.32	16
15	Middle Aterno Valley 1	0.43	0.33-0.53	0.47	14
16	Middle Aterno Valley 2	0.16	0.01-0.47	2.80	1
17	San Sebastiano	0.35	0.26-0.45	0.55	11
18	Ventrino	0.55	0.41-0.71	0.54	7
19	Parasano	0.46	0.38-0.54	0.34	20
20	San Benedetto-Gioia dei Marsi 1	0.51	0.43-0.60	0.34	19
21	San Benedetto-Gioia dei Marsi 2	0.83	0.51-1.35	1.01	1
22	Bacinetto	0.38	0.08-1.10	2.66	1
23	Trasacco	0.29	0.22-0.36	0.48	20
24	Luco dei Marsi	0.31	0.03-0.88	2.74	1
25	Tre Monti 1	0.29	0.22-0.36	0.50	17
26	Tre Monti 2	0.20	0.05-0.37	1.62	2
27	Magnola	0.64	0.58-0.71	0.19	42
28	Liri 1	0.98	0.65-1.43	0.80	2
29	Liri 2	0.82	0.68-0.98	0.37	8
30	Barisciano-San Pio delle Camere 1	0.37	0.24-0.52	0.77	4
31	Barisciano-San Pio delle Camere 2	1.02	0.69-1.40	0.70	3
32	Paganica	0.23	0.18-0.28	0.44	23
33	San Demetrio	0.37	0.25-0.49	0.64	4
34	Middle Aterno northern splay 1	0.08	0.00-0.26	3.21	1
35	Middle Aterno northern splay 2	0.39	0.08-1.17	2.82	1
36	Ovindoli-Pezza	0.81	0.65-0.99	0.42	26
37	Campo Felice	0.74	0.68-0.81	0.18	39
38	Campo Felice-northern splay	0.97	0.71-1.23	0.53	1
39	Campo Felice-Colle Cerasitto 1	0.21	0.08-0.39	1.47	5
40	Campo Felice-Colle Cerasitto 2	0.31	0.18-0.46	0.89	4
41	Velino 1	0.85	0.59-1.01	0.49	7
42	Velino 2	0.43	0.15-1.09	2.21	1
43	Scurcola	0.44	0.29-0.60	0.72	6

44	Carsoli	0.36	0.26-0.49	0.63	6
45	Campo Imperatore 1	0.94	0.62-1.31	0.73	3
46	Campo Imperatore 2	0.80	0.65-0.94	0.37	5
47	Campo Imperatore 3	0.26	0.13-0.40	1.05	5
48	Assergi 1	0.21	0.03-0.55	2.45	1
49	Assergi 2	1.09	0.75-3.08	2.15	1
50	Montecristo 1	0.32	0.07-0.69	1.97	1
51	Montecristo 2	0.26	0.04-0.61	2.20	1
52	Mt. San Franco	0.84	0.50-1.47	1.16	1
53	Stabiata	0.47	0.19-0.91	1.54	1
54	Pettino	0.64	0.40-0.90	0.79	1
55	Pizzoli	0.42	0.29-0.57	0.64	4
56	Sella di Corno	0.31	0.14-0.49	1.13	3
57	Fiamignano	0.98	0.77-1.23	0.46	9
58	Leonessa	0.39	0.21-0.64	1.09	2
59	Rieti	0.32	0.14-0.55	1.26	2